Case Studies in Thermal Engineering 50 (2023) 103513

Contents lists available at ScienceDirect

Case Studies in Thermal Engineering

journal homepage: www.elsevier.com/locate/csite

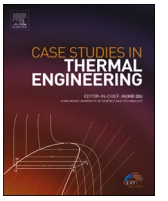

# Effect of diameter, twist angle, and blade count on the thermal-hydraulic performance of a decaying twisted swirler

At-Tasneem Mohd Amin [a,*], Wan Azmi Wan Hamzah [a,b], Mohd Azmi Ismail [c]

[a] Faculty of Mechanical and Automotive Engineering Technology, Universiti Malaysia Pahang Al-Sultan Abdullah, 26600, Pekan, Pahang, Malaysia
[b] Centre for Research in Advanced Fluid and Processes, Lebuhraya Tun Razak, Kuantan 26300, Pahang, Malaysia
[c] School of Mechanical Engineering, Universiti Sains Malaysia Engineering Campus, 14300, Nibong Tebal, P. Pinang, Malaysia

ARTICLE INFO

*Keywords:*
Heat transfer enhancement method
Friction factor
Thermal-hydraulic performance
Swirler
Turbulator

ABSTRACT

Inserting a decaying swirler into a heat exchanger has been shown to improve heat transfer with minimal effect on the friction factor. The study analyses the effect of diameter, twist angle, and blade count on the thermal-hydraulic performance of a Decaying Twisted Swirler (DTS) in a horizontally heated tube. The diameter, twist angle, and DTS's blade count are examined for 13.5 mm–15.5 mm with a 0.5 mm interval, 0°–360° with a 60° gap, and 2 to 6 blades, respectively. The Nusselt number, friction factor, and thermal-hydraulic performance are examined for Reynolds numbers between 4583 and 35000. The relative Nusselt number and friction factor increase as DTS diameter and twist angle increase, reaching a maximum value at Re = 4583. Despite this, the relative Nusselt number dispersed as the blade count increased. The relative friction factor increases as the blade count increases. Maximum relative Nusselt number and friction factor reached 1.64 and 3.25, respectively with DTS's 15.5 mm diameter, 360° angle, and 4 blades. Nonetheless, the thermal-hydraulic performance is greatest when the DTS has a diameter of 15.5 mm, a twist angle of 180°, and 2 blades with 1.17.

**Nomenclature**

| | |
|---|---|
| $C_p$ | Specific heat, J/kg·K |
| CFD | Computational fluid dynamics |
| D | Diameter, m |
| DTS | Decaying Twisted Swirler |
| d$P$ | Pressure difference, Pa |
| EG | Ethylene glycol |
| $f$ | Friction factor |
| $h$ | Heat transfer coefficient, W/m$^2$·K |
| HVAC | Heating, ventilation, and air conditioning |
| $I$ | Initial turbulent intensity |
| $k$ | Thermal conductivity, W/m·K |
| L | Length, m |

* Corresponding author.
*E-mail address:* tasneem@ump.edu.my (A.-T. Mohd Amin).

https://doi.org/10.1016/j.csite.2023.103513
Received 24 July 2023; Received in revised form 15 September 2023; Accepted 19 September 2023
Available online 20 September 2023

| | |
|---|---|
| *Nu* | Nusselt number |
| PEC | Performance evaluation criteria |
| $\dot{q}$ | Heat flux, W/m$^2$ |
| RANS | Reynolds-Averaged Navier-Stokes |
| Re | Reynolds number |
| RNG | Renormalisation group |
| RSM | Reynolds stress model |
| SIJ | Swirling impinging jet |
| SST | Shear stress transport |
| *T* | Temperature, K |
| THP | Thermal-hydraulic performance |
| *V* | Velocity, m/s |
| VG | Vortex generator |
| W | water |

*Greek symbols*

| | |
|---|---|
| μ | Dynamic viscosity, Pa·s |
| ρ | Density, kg/m$^3$ |

*Subscripts*

| | |
|---|---|
| *b* | Bulk |
| *in* | Inlet |
| *max* | Maximum |
| *rel* | Relative |
| *s* | Surface |
| *SG* | Swirler |
| *PT* | Plain tube |

**Table 1**
Various types of swirlers.

| Type of SG | Authors | Name of SG | Method of Study | Flow Regime |
|---|---|---|---|---|
| Surface modification | Firoozi et al. [32] | Dimple configuration | Numerical (SST $k-\omega$) | Laminar to Turbulence (Re = 500–4000) |
| | Du et al. [33] | Transversely mounted sinusoidal ribs | Experiment | Laminar: (Re = 400–1800) |
| | Bellos et al. [34] | Internal rectangular fins | Numerical | Turbulence (Re = 5000–130000) |
| | Zheng et al. [35] | Vortex rods | Numerical | Laminar (Re = 300–1800) |
| | Zheng et al. [36] | Parallel-type ribs and V shape type ribs | Numerical (shear stress tensor $\kappa-\omega$, SST-$\kappa-\omega$) | Turbulence (Re = 6000–21000) |
| | Jedsadaratanachai et al. [37] | 45 °V-baffles | Numerical | Laminar (Re = 100–2000) |
| | Promvonge et al. [38] | 30° inclides vortex rings | Experiment | Turbulence (Re = 5000–26000) |
| Continuous swirler | Goh et al. [39] | Self-rotating generator insert | Experiment | Turbulence (Re = 10000–24000) |
| | Liu et al. [40] | Fluid exchange insert | Numerical | Laminar (Re = 100–500) |
| | Pourramezan et al. [41] | Twisted conical strip inserts | Numerical | Laminar |
| | Nakhchi et al. [42] | Perforated louvered strip insert | Numerical (k-epsilon RNG) | Turbulence (Re = 5000–14000) |
| | Mashayekhi et al. [43] | Two rows of twisted conical strip inserts | Numerical (two-phase mixture model) | Laminar (Re = 250–1000) |
| | Bahiraei et al. [44] | Twisted conical strip insert | Numerical | Laminar (Re = 460–2300) |
| | Alimoradi et al. [45] | Transversely twisted-generators | Experiment + Numerical | Laminar (Re = 1500–5000) |
| Decaying swirler | Saedodin et al. [25] | Twisted turbulator | Numerical | Laminar (Re = 4125–5363) |
| | Indurain et al. [26] | Swirler with profiled blades | Numerical (SST $k-\omega$) | Turbulence (Re = 10000–200000) |
| | Yan et al. [46] | Multi-lobed swirler | Numerical (RSM) | Turbulence (Re = 50000–125000) |
| | Nikoozade et al. [47] | Propeller turbulator | Numerical (SST & two-phase mixture model | Turbulence (Re = 5000–30000) |
| | Xu et al. [27] | Winglet vortex generator | Numerical | Turbulence (Re = 6000–33000) |
| | Jumpholkul et al. [28] | Free-rotating swirler | Experiment | Turbulence (Re = 3500–13000) |
| | Jafari et al. [29] | Four-point star swirler | Experiment | Turbulence (Re = 12000–27000) |
| | Taheran et al. [30] | 6 blades swirl flow generator | Numerical and Experiment | Turbulence (Re = 4000–10000) |

## 1. Introduction

A heat exchanger is a device that transfers heat from one medium to another of varying temperatures. It used in various industries, including automotive sectors such as car radiators, chemical, petrochemical and oil and gas industries such as steam condensation or pre-heating the inlet fluid of a boiler, food industries, manufacturing industries, and refrigeration industries [1]. Furthermore, it is beneficial for human daily life applications such as air conditioners, shell and tube heat exchangers, heaters, furnaces, cooling towers, solar collectors, refrigerators, heating, ventilation, and air conditioning equipment (HVAC) [2]. These heating and cooling operations consume a lot of energy and worsen climate change [3]. As a result, there has been a surge in research into heat transfer enhancement techniques, emphasising energy conservation and environmental protection. The study aims to improve the thermal-hydraulic performance (THP) of existing heat exchangers, reduce heat exchanger size while maintaining heat transfer performance, upgrade operational processes, and/or conserve pumping power. In fact, three unique heat transfer enhancement methods exist: passive, active and compound methods. The active method requires external power, the passive method does not, and the compound method combines the two methods [4]. All methods are proposed to create turbulent flow, which optimises the interaction of molecules at higher and lower temperatures and improves heat transfer. Many active methods have been documented in the literature, including the effects of an electrostatic field [5], swirling impinging jet (SIJ) [6], superimposing of transverse mechanical oscillation [7,8], and magnetic field swirling flow [9]. On the other hand, passive methods necessitate nanoparticle dispersion [10–14], swirler inserts [15–17], or pipe wall surface modification to disturb the flow and generate turbulence.

Focusing on the passive method using swirler inserts, a swirler is a device that has been imparted in the flowing fluid to generate a swirl velocity component, which is the velocity circumferential and axial component [18]. The swirler is also known as the swirl generator or turbulator in the literature. Swirl flow works to thin the thermal boundary layer, allowing for greater heat transfer from the warmer to the cooler medium. It is beneficial in turbomachinery, pollution control devices, combustion chambers, fusion reactors, and other similar applications [19]. There are three types of swirlers: tube' surface modification [20–22], continuous [23,24] and decaying swirlers. The surface of a smooth tube is modified in such a way as to extend the area that is subjected to heat transfer. On the other hand, a continuous swirler is inserted along the tube to maintain the swirling flow along the test section. In contrast, a decaying swirler is placed in a specific location to induce the swirling flow, and the generated swirl flow disappears after a certain distance downstream. Table 1 shows tabulated examples of a few types of swirlers that have been numerically and experimentally explored in various flow regimes. Aside from the extensive research into various designs of continuous swirlers such as twisted and helical tape, twisted tube, conical rings, plate inserts, wired coil and array generators, and various surface modifications, each design has also widely documented the effect of different parameters and modifications with the goal of increasing THP. Unlike the continuous swirler, the decaying swirler is still accessible to diverse design exploration.

As shown in Table 1, many designs of decaying swirlers have been proposed in the literature for these purposes. Saedodin et al. [25], Indurain et al. [26], and Xu et al. [27] numerically investigated the existence of a decaying swirler in a heated tube for its thermal performance. Saedodin et al. [25] simulated the various metal oxide nanofluids flowing through a twisted turbulator with six blades twisted to 180°. Indurain et al. [26] investigated the thermal performance of air through an axial guide vane swirler with eight profiling blades. These blades are attached to the wall at an exit angle of 40°. Xu et al. [27] attached a winglet vortex generator to the tube inlet wall. Four vortex generators were attached to the tube wall at four different angles with three different blockage ratios to find the optimum combination of both parameters that give maximum thermal performance. On the other hand, Jumpholkul et al. [28], Jafari et al. [29] and Taheran et al. [30] investigated thermal performance through experiments. The swirlers were designed, fabricated, and inserted in the heated tube with selected nanofluids used as a working fluid.

Unlike continuous swirlers, the swirling flow generated by decaying swirlers at the upstream flow will eventually decay due to viscosity and friction. The location of the swirler inserts and the length of the heated tube are essential to identify the survivability of the swirling flow as the thermal performance is evaluated along the tube. Thermal-hydraulic performance (THP) evaluates decaying swirlers' thermal performance. THP is also known as heat exchangers' performance evaluation criteria (PEC) or efficiency index in the literature. THP is a measure of heat transfer enhancement under a particular pumping power that employs the overall performance of the swirler inside the tube. Equation (1) is used to determine THP [31].

$$THP = \frac{Nu_{rel}}{(f_{rel})^{\frac{1}{3}}} \tag{1}$$

where $Nu_{rel}$ and $f_{rel}$ are determined as follows:

$$Nu_{rel} = \frac{Nu_{SG}}{Nu_{PT}} \tag{2}$$

and

$$f_{rel} = \frac{f_{SG}}{f_{PT}} \tag{3}$$

where $Nu_{SG}$ is a Nusselt number of the flow when the swirler was inserted in the tube, $Nu_{PT}$ is the Nusselt number of the flow of the plain tube, $f_{SG}$ is a friction factor of the flow when the swirler is inserted in the tube and $f_{PT}$ is the friction factor of the flow of the plain tube. The Darcy friction factor, $f$ is computed in Equation (4).

$$f = dP\frac{D}{L}\frac{2}{\rho V^2} \tag{4}$$

where $dP$ is the pressure difference between the tube flow's inlet and outlet. The Nusselt number, $Nu$ was measured locally, and the average for the whole investigated points is calculated in Equation (5).

$$Nu = \frac{hD}{k} \tag{5}$$

where $k$ is the thermal conductivity of the working fluid and convective heat transfer coefficient, $h$ is calculated in Equation (6).

$$h = \frac{\dot{q}}{(T_s - T_b)} \tag{6}$$

where $\dot{q}$ is a constant heat flux applied along the plain tube, $T_s$ and $T_b$ are wall surface temperature and bulk temperature of the flow, respectively.

Several decaying swirlers were tested in a horizontally heated tube, summarising their maximum performances in Table 2.

The same goal has been proposed for various designs, each of which varies the dimensions of the swirler and test section, working fluids, twist angle and blade count to generate a strong swirling flow. Since the swirling flow eventually decays after travelling a certain distance downstream, the location of the swirler and the length of the test section are critical in determining how long the swirling flow can persist. Therefore, the shorter dimensionless length of the test section was listed at the top of the table. All tests were conducted in turbulent flow conditions. The maximum $Nu_{rel}$ is highest for the shortest test section and decreases as the test section length increases because of the swirling flow's intensity level. However, the $f_{rel}$ varies depending on the swirler design and blockage area. Consequently, the THP varies for all swirlers. Jumpholkul et al. [28] obtained the highest THP by incorporating a free-rotating swirler with a 90° twist angle tested at a $SiO_2$/water concentration of 2.0 vol% and a temperature of 35°C. Despite the test section being the longest item on the list, the THP is the highest.

This work continues the investigation by Abdul Hamid et al. [49] of the heat transfer performance of a continuous swirler named wire coil insert in a horizontal heated tube. The experiment used a working fluid consisting of a 60:40% water and ethylene glycol mixture. The wire coil was evaluated for a Re range of 2300–12000. The THP is greater than one, with an increase in heat transfer efficiency of up to 254.4%. However, the friction factor increased to be up to 6.38 times higher than a plain tube, necessitating an exponentially greater pumping power. Consequently, the purpose of this paper is to evaluate the potential of a decaying swirler numerically to minimise the impact on the pumping capacity in the same test section. The decaying swirler is called the Decaying Twisted Swirler (DTS). The geometry and parameters of the DTS were meticulously designed to generate the greatest swirl flow with the least possible flow obstruction. Simultaneously, the design's complexity, size, and thickness of the DTS were carefully considered to 3D print the DTS with excellent surface quality and durability for experimental testing.

## 2. Numerical modeling

### 2.1. Computational domain

This simulation's computational domain was adapted from an experiment by Abdul Hamid et al. [49]. A three-dimensional copper circular, straight tube in horizontal orientation with a diameter of 0.016 m and a length of 1.5 m or length over diameter, L/D = 93.75, was modelled using Solidwork 2021. Fig. 1 displays the computational domain of the simulation. The domain was divided into three sections for mesh independent test: the entrance, swirler and test sections. The entrance length is 0.155 m or L/D = 10. The length of the generator section is 45 mm or L/D = 2.8, with the DTS located at the center of the section. The length of the test section is 1.3 m,

**Table 2**
Performance of decaying swirlers.

| Authors | L/D SG | L/D tube | Working fluid | Twist angle | Blade count | Investigations | Max $Nu_{rel}$ | Max $f_{rel}$ | THP |
|---|---|---|---|---|---|---|---|---|---|
| Jafari et al. [29] | 1.0 | 3.00 | W:EG mixture | 90°, 180°, 270°, 360° | 4 | W: EG volume ratio & twist angle | 1.75 | 1.6 | 1.54 |
| Indurain et al. [26] | 0.5 | 5.00 | Air | – | 8 | SG performance | 1.57 | 3.9 | >1 |
| Xu et al. [27] | – | 5.38 | Air | – | 4 | Attach angles & blockage ratios | 1.75 | 1.3 | 1.3 |
| Nikoozade et al. [47] | 0.2 | 34.70 | $Al_2O_3$/water | – | 6 | SG performance & nanofluids concentration | 1.28 | 1.7 | – |
| Bilen et al. [48] | 5.5 | 45 | Air | 0°, 22.5° 41° 50° | 4 | Twist angle | 1.41 | 6.76 | 0.83 |
| Saedodin et al. [25] | 16.7 | 83.30 | $Al_2O_3$, CuO, $TiO_2$, $SiO_2$/water | – | 6 | SG performance & nanofluids concentration | 1.08 | 1.1 | 1.06 |
| Jumpholkul et al. [28] | 3.2 | 281.00 | $SiO_2$/water | 30°, 60°, 90° | 4 | Inlet temp, twist angle & nanofluids concentration | 1.54 | 1.2 | 1.7 |

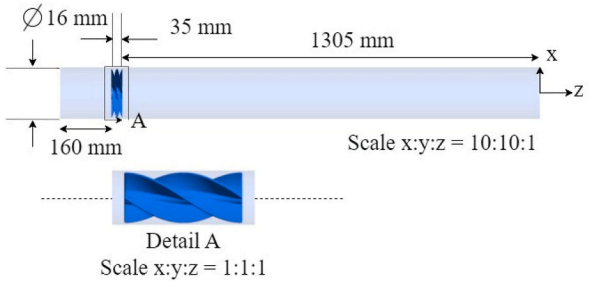


**Fig. 1.** Computational domain.

where the analysis of swirl generation will be conducted. The physical properties of the copper tube are tabulated in Table 3.

### 2.2. Swirler geometry

The Decaying Twisted Swirler (DTS) is designed and inspired by twisted tape, a typical continuous swirler. Although the twisted tape outperformed the plain tube in terms of THP by up to 2.5 times, the friction factor increased by 350% [50]. As a result, it is recommended that the DTS be positioned at the entrance of a fully developed flow region, which is at L/D = 10. This point is sufficient to allow uniform inlet velocity flows before entering the fully developed section of a plain tube. DTS will aid in generating swirl flow while having a minimum impact on the friction factor. The DTS has a length of 35 mm or L/D = 2.25. The short length of the DTS was designed to reduce surface friction between the generator's wall and the fluid. To begin the parametric study, the diameter of the DTS is set to 15.5 mm, which is 3% less than the diameter of the tube. It has four blades with a thickness of 1 mm that guide the flow with the least drag. The DTS twist angle of 180° is designed to provide a high swirl intensity that lasts as long as possible in the test section. Then, Nusselt number, friction factor and thermal-hydraulic performance are tested for a range of diameter, twist angle and blade count. The parameters and isometric view of DTS are given in Table 4 and Fig. 2, respective.

Similar to the experiment, water and ethylene glycol mixture, in a ratio of 60:40%, serves as the working fluid in this numerical simulation. Its thermophysical properties and heat transfer performance are superior to its constituent working fluids [51]. The thermophysical characteristics of W: EG 60:40% are listed in Table 5.

### 2.3. Mesh characterisation

Fig. 3 illustrates the mesh generation for the geometry domain. The fluent mesh was used to generate a multi-block mesh for three separate sections, the entrance, the swirler, and the test section of the tube. All meshes were created using Ansys Fluent Mesh. The hexahedral cell's structured mesh is for the entrance and test sections. For simplicity, the unstructured mesh of the tetrahedral mesh is generated for the swirler's section. The global mesh size is 0.6 mm. The smooth transition of 15 layers of inflation was developed along the tube with a growth rate of 1.15.

### 2.4. Governing equation

The transport equation was used to solve the fluid's convection and diffusion terms. The convection term reflects thermal energy transport by the motion of a moving fluid. In contrast, the diffusion term denotes thermal energy transport from a higher to a lower temperature due to a temperature difference between two spaces. CFD Fluent simulated a three-dimensional, incompressible, steady turbulent flow with Re ranging from 4583 to 35000. The RANS turbulence model is used in CFD Fluent to considerably minimise the time and computing effort required to resolve complex geometry down to the smallest scale of motion in a turbulence structure.

Nevertheless, RANS introduces six additional terms in the transport equation which are Reynolds stresses tensor, $-\rho\langle uiuj\rangle$, which requires closure equations to solve them. Reynolds Stress Model (RSM) is a turbulence model that predicts various turbulence structures such as streamlined curvature, swirl, rotation, and rapid changes in strain rate by using individual Reynolds stresses $< u_i' u_i' >$ and dissipation rate [53]. It has seven equations that simulate these structures more extensively than any one or two-equations models, allowing it to accurately represent the turbulence characteristics that occur downstream of the DTS. Furthermore, the convective heat transfer coefficient, $h$ is highly dependent on the near-wall values, and the core region flows [54]. Even though the flow thermal features differ significantly between the wall viscous and core regions, RSM computed the wall adjacent cells using the local turbulence fluctuation and computed globally with the RSM for flow at the core region for computational convenience. Yan et al. [55] also used RSM to numerically evaluate a decaying multi-lobed swirler inserted in a plain horizontal tube because it has a higher level of computational refinement than any other Reynolds Average Navier-Stokes (RANS) model.

**Table 3**
Thermophysical properties of copper tube.

| Properties | Value |
|---|---|
| Thermal conductivity, $k$ [W/m·K] | 387.6 |
| Density, $\rho$ [kg/m$^3$] | 8978 |
| Specific Heat, $C_p$ [J/kg·K] | 381.0 |

**Table 4**
Parameters of DTS.

| Description | Parameter |
|---|---|
| Diameter [mm] | 15.5, 15.0, 14.5, 14.0, 13.5 |
| Twist angle | 0°, 60°, 120°, 180°, 240°, 300°, 360° |
| Blade count | 2, 3, 4, 5, 6 |

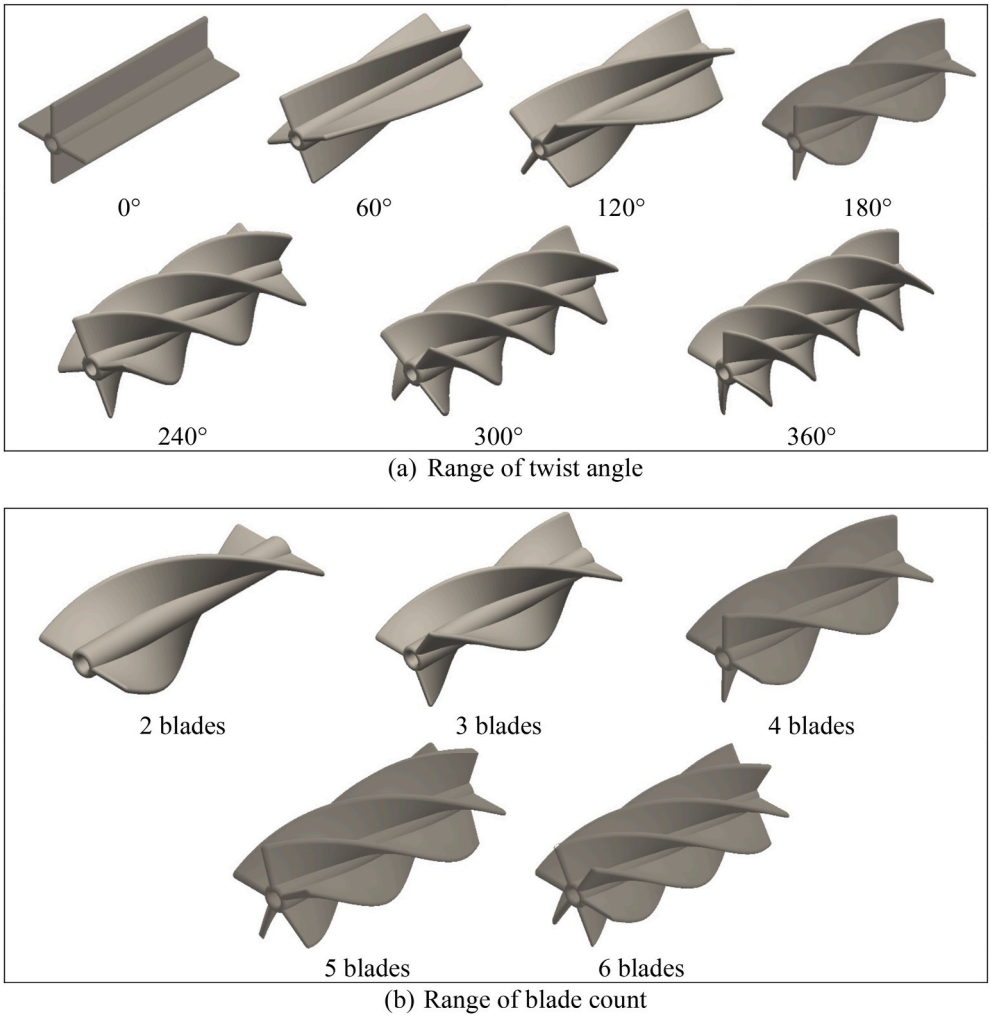


**Fig. 2.** Isometric view of DTS.

**Table 5**
Thermophysical properties of W: EG 60:40% at 29 °C [52].

| Properties | Value |
|---|---|
| Thermal conductivity, $k$ [W/m·K] | 0.4112 |
| Density, $\rho$ [kg/m$^3$] | 1055.832 |
| Dynamic viscosity, $\mu$ [Pa·s] | 0.002322 |
| Specific heat, $C_p$ [J/kg·K] | 3498.6 |

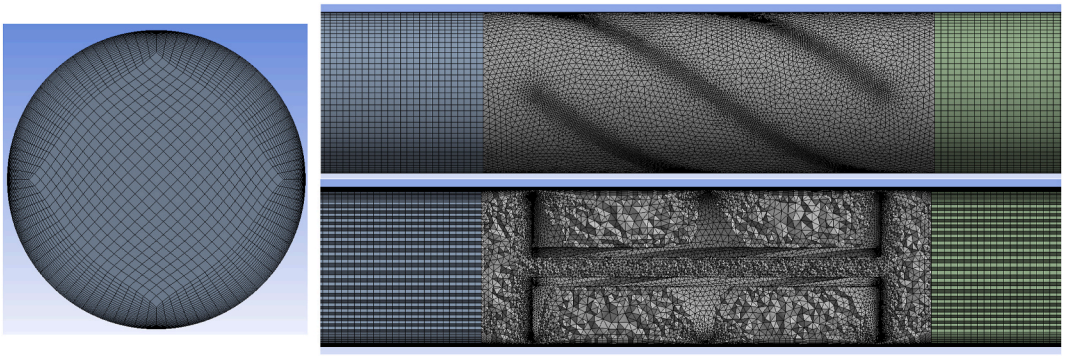

**Fig. 3.** Mesh generation.

An Ansys Fluent 2020 R1 software was used to simulate in conjunction with an AMD Ryzen 9 3950X 16-Core Processor at 3.49 GHz and 128 GB of installed RAM.

### 2.5. Boundary conditions

Fig. 4 and Table 6 show the boundary conditions for the tube's inlet, outlet, and wall conditions, as well as the swirler. For RSM model, the individual Reynolds stresses require additional inlet boundary conditions, which are the initial turbulent intensity, $I$ and characteristic length, $l$. The characteristic length for the horizontal tube is the diameter of the tube, 0.016 m. The flow's turbulent intensity at core region is estimated using Equation (7) [56].

$$I = 0.16\, Re^{-\frac{1}{8}} \tag{7}$$

### 2.6. Mesh independent test

A mesh independent test was performed to identify the optimum mesh configuration to ensure the simulation results are independent of the mesh size. Table 7 summarises the details of the mesh independent test.

The global mesh size of the plain tube was tested at a size ranging from 2 mm to 0.4 mm. The configuration of layer inflations was investigated for 15 and 20 layers at the same global mesh size to analyse the change in parameters at the wall and core region. Throughout the test, the growth rate of inflation layers was kept constant. As a result, the number of cells generated ranges from 303912 to 9238775, labelled as Mesh 1 until Mesh 7. The friction factor, Nusselt number, and maximum W: EG flow velocity in a horizontal heated tube were compared using experimental data from Abdul Hamid et al. [49] and empirical correlations. The friction factor was compared to the equations of Blasius [58], Petukhov [59] and Colebrook-white [60]. The Nusselt number was compared using the Dittus-Boelter [61] and Gnielinski [62] equations. The result of the mesh independent test is presented in Section 3.1.

## 3. Results and discussion

The purpose of this simulation is to investigate the effect of DTS on the THP in a horizontal heated tube. A turbulent flow of Re ranging from 4583 to 35000 was simulated. After presenting the results of a mesh-independent test for a plain tube, the swirl flow generated when the base fluid passed through a DTS with a diameter of 15.5 m, an angle of 180°, and 4 blades is visualized. The friction factor, Nusselt number, and THP for this parameter are then presented. The DTS is then investigated further to determine the effect of DTS diameter, twist angle, and blade count. The optimal parameter that yielded the greatest THP will be determined through this investigation. A comparison of the performance of the DTS with that of other swirlers is presented before suggestions are made regarding further investigation into the DTS.

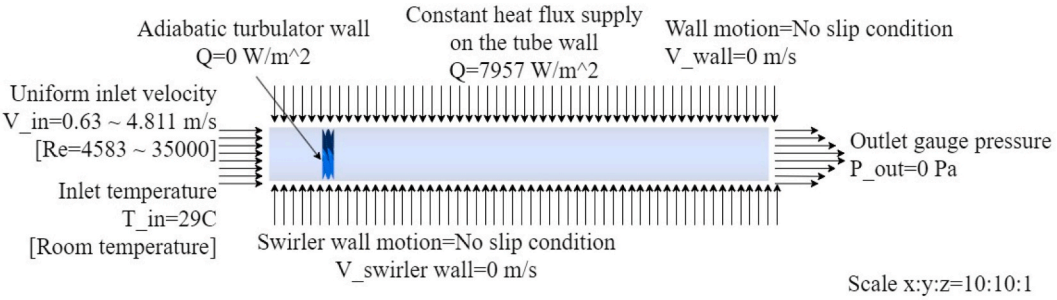


**Fig. 4.** Boundary condition.

**Table 6**
Boundary conditions.

| Descriptions | | Value |
|---|---|---|
| **Inlet Conditions** | Velocity magnitude, $V_{in}$ [m/s] | : 0.630–4.811 [Re = 4583–35000] |
| | Inlet temperature, $T_{in}$ [°C] | : 29 |
| | Initial turbulence intensity, $I_{in}$ (%) | : 5.58–4.33 |
| **Wall** | No slip conditions | : 7957 |
| | Uniform constant heat flux [W/m$^2$] | |
| **Swirler** | No-slip conditions | : 0.681 W/m$^2$ [57] |
| | Adiabatic wall [Resin] | |
| **Outlet Conditions** | Pressure [Pa] | : 0 |

**Table 7**
Details of mesh independent test.

| Mesh number | Mesh Size [mm] | Number of Layer Inflation | Growth rate | Number of Cells |
|---|---|---|---|---|
| 1 | 2 | 15 | 1.15 | 303912 |
| 2 | 1 | 15 | 1.15 | 1344733 |
| 3 | 0.8 | 15 | 1.15 | 2123136 |
| 4 | 0.8 | 20 | 1.15 | 2681856 |
| 5 | 0.6 | 15 | 1.15 | 3888486 |
| 6 | 0.6 | 20 | 1.15 | 4848606 |
| 7 | 0.4 | 15 | 1.15 | 9238775 |

### 3.1. Mesh independent test

The mesh independent test is essential in any simulation study because it identifies the optimal mesh size and layer of inflation configuration which reflect the total number of cells the computer must process during the simulations. The number of cells must be reasonable to be consistent with the computer's capacity, capabilities, and acceptable running time. The mesh independent test was carried out for seven different meshes configurations by increasing the cell number from 303912 to 9238775. It was conducted for Re of 4583 and 10136. The optimal mesh configuration is chosen when the friction factor and Nusselt number are nearly constant as the number of cells increases.

Fig. 5 shows the friction factor, Nusselt number, and velocity maximum for force convection simulation along a circular tube with a low number of cells to the highest number of cells for Re of 4583 and 10136. The selected mesh was then tested for an extended range of Re, up to 35000.

Fig. 5a-c demonstrated that when the number of cells rose from Mesh 1 to Mesh 7, $f$ declined, $Nu$ increased and $V_{max}$ increased for both Re of 4583 and 10136. Nonetheless, when the mesh increased by 3584574 from Mesh 1 to Mesh 5, $f$ decreased twice as much as it did by 5350289 from Mesh 5 to Mesh 7. The same can be said of the Nusselt number for both Re. The maximum velocity for both Re increased significantly as the number of cells increased, eventually stopping at Mesh 5. Despite an increase in the number of cells of around 1 million from Mesh 5 to Mesh 6, there is no discernible effect on $f_{rel}$ for Re of 10136, and at both Re for $Nu$ and $V_{max}$. As a result, Mesh 5 is recommended for the continuation of the simulation.

The results of the simulation of Mesh 5 are then compared to experimental data collected by Abdul Hamid et al. [49] for the plain tube, as well as empirical results of friction factor by Blasius [58], Petukhov [59] and Colebrook-white [60] and Dittus-Boelter [61] and Gnielinski [62] equations for Nusselt number. The result indicates that the friction factor trend is consistent with all experimental and empirical findings. Despite this, due to the number of cells employed in the simulation, the data is slightly higher than the comparison data, where the deviation errors between the simulation, experiment, and all empirical equations are 10% for friction factor and 1% for Nusselt number. As the number of cells increased, the friction factor became more congruent with empirical and experimental data slops. Unfortunately, achieving that state is computationally intensive. However, the presence of DTS will be modelled here to show how heat transfer is enhanced and the friction factor is increased compared to a plain tube. Consequently, the disparity in error between the result and the comparative data will be eliminated. Thus, the numerical modelling settings are sufficient for this simulation.

### 3.2. Decaying twisted swirler performance

#### 3.2.1. Flow visualization

Fig. 6 shows the streamline, vortex core, and contour plot of the velocity circumferential along the tube after W: EG passed through the DTS at the lowest and highest Re observed, respectively. As mentioned ealier, this is the performance for DTS' diameter of 15.5 mm, 180° and 4 blades. Since the generator was positioned at L/D = 10 from the inlet, the dynamic change in velocity circumferential can be seen in the figures beginning from this point forward. The flow was configured to be uniform at the inlet, as shown in green in the figure. High-velocity regions are depicted in orange, whereas decreasing velocities are represented by a gradual transition from orange to yellow to green to blue.

As illustrated in Fig. 6a, when the flow approached the leading edge of the generator at Re of 4583, the streamline was distorted towards the twisted angled wall due to the presence of the DTS. As the flow travels along the swirler, its velocity increases, causing the

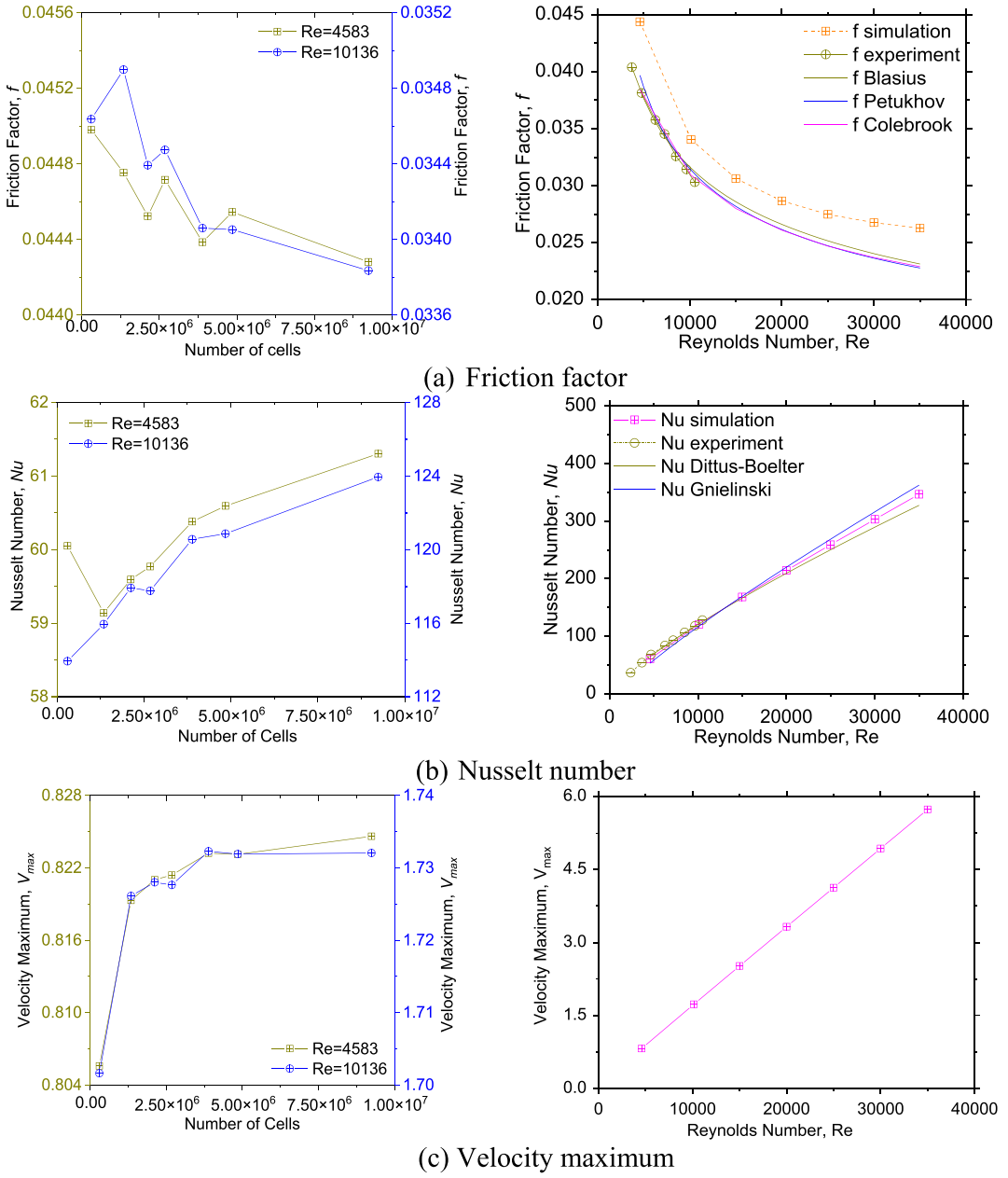


**Fig. 5.** Mesh independent test.

velocity circumferential of the flow to develop and a swirling flow to form. As the velocity inside the DTS increases, the pressure in the plain tube drops drastically, beginning at the leading edge of the DTS and continuing until it exits the generator, as shown in Fig. 7. The swirling flow was formed after passing through the tube's trailing edge downstream of the DTS. Fig. 6 also reveals the presence of turbulence structure of swirling flow for both Re of 4583 and 35000. The swirling strength is most remarkable as it leaves the generator's trailing edge. Since this swirling intensity is strongest at this moment, the pressure is minimal until the swirling strength is progressively weakened as it travels downstream and the pressure is restored. After 0.8 m downstream or L/D = 62.5, the strength of the swirling flow finally fades.

As the Re increases, the uniform inlet velocity and pressure also increase. As presented in Fig. 6b, the flow's velocity that approached the leading edge of the DTS was substantially increased as the streamline was distorted by the twisted angled wall of the generator and the swirling flow created. The turbulent structure becomes more pronounced as the flow exits the generator. As the velocity circumferential increases, the swirl intensity is stronger at the vortex's inner core. The generator maintained the swirl intensity for the first 0.3 m downstream (L/D = 12.5 to 31.25). The pressure at this point is drastically dropped at this location. Since the velocity is greater at higher Re, the swirling strength has more momentum to survive across longer distances than at lower Re. As it

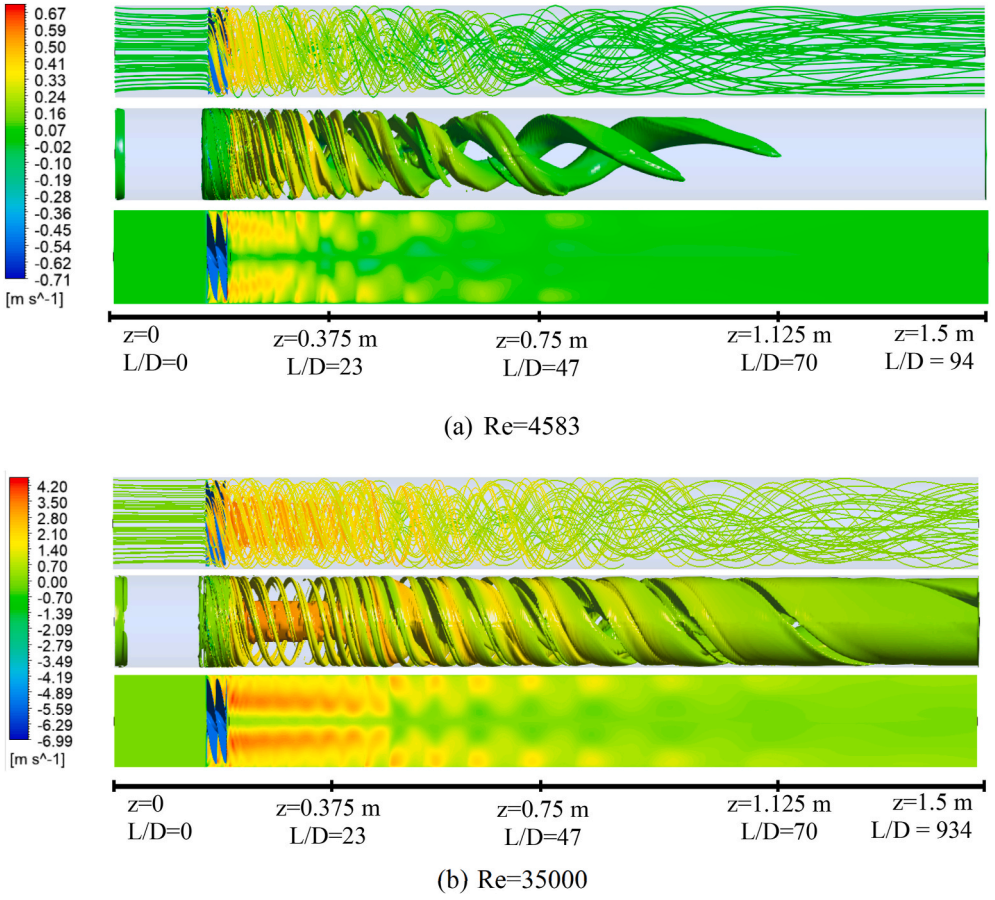


**Fig. 6.** Streamline (top), vortex core of swirl strength (middle) and contour plot of velocity circumferential (bottom) at lowest and highest investigated Reynolds number (Figure scale x: y: z = 10: 10:1).

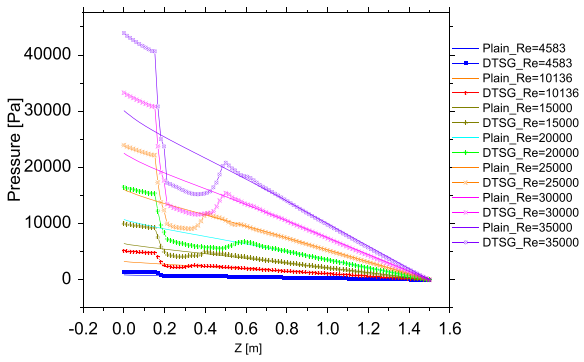


**Fig. 7.** Pressure along the tube.

moves downstream, the swirling flow gradually loses momentum. Hence, the swirling flow dissipated completely after L/D = 75.

### 3.2.2. Friction factor

The pressure difference is utilized to determine the Darcy friction factor (Equation (4)) and the $f_{rel}$ (Equation (3)) of the heated tube with a DTS insert, as displayed in Fig. 8. As the Re increases in a plain tube, the friction factor reduces. A similar trend was observed for the DTS insert in the tube with respect to the Re as was observed for the plain tube. The friction factor of the fluid with the DTS insert inside the tube increases at all Re compared to the plain tube. Hence, the $f_{rel}$ follows the same trend, with the maximum value recorded at the lowest Re of 4583 and dropping steadily as the Re increases. The maximum relative friction factor is 1.64, and the lowest is 1.47. The boundary layer thickness developed on the pipe's wall surface is thicker at a low Re than at a high Re. When the presence of DTS

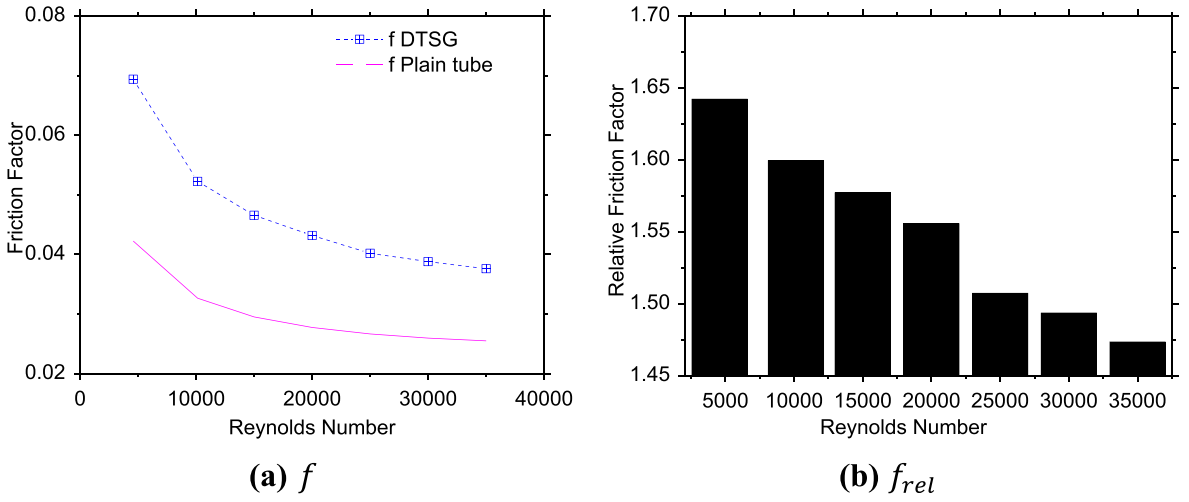


**Fig. 8.** Friction factor of Decaying Twisted Swirler.

obstructed the inlet flow, the fluid flow experienced pressure drag and surface friction drag on the DTS's blockage. The pressure drag is comparable at both low and high Re because the geometry and size of DTS are the same. However, because the surface friction drag is stronger at low Re than at high Re, the overall drag is greater at low Re than at high Re, resulting in a larger friction factor.

### *3.2.3. Nusselt number*

The constant heat flux was supplied to the plain tube, and the inlet temperature of W: EG was 302.15 K. Fig. 9 shows the wall and centerline temperature of the plain tube, and a plain tube with DTS inserts in all investigated Re. As heat flux was supplied to the tube wall, the wall temperature increased relative to the centerline temperature, resulting in heat convection. Fig. 9a shows that as W: EG flows downstream along the heated tube, the wall and centerline's temperature progressively increase. At the same time, as the Re increases, both the wall and centerline temperatures decrease. DTS was inserted into the flow to form a swirling flow that imparts energy to fluid particles and improves the interaction between centerline fluid and fluid near the wall. Since the swirl flow formed on the trailing edge of the DTS, the wall temperature is dramatically reduced when fluid passes through the DTS, as presented in Fig. 9b. The molecules at the centerline has become intrinsically intertwined with the molecules with higher temperature at the wall. As the fluid flows downstream, the swirling strength weakens, and heat transfer from the centerline to the wall temperature reduced

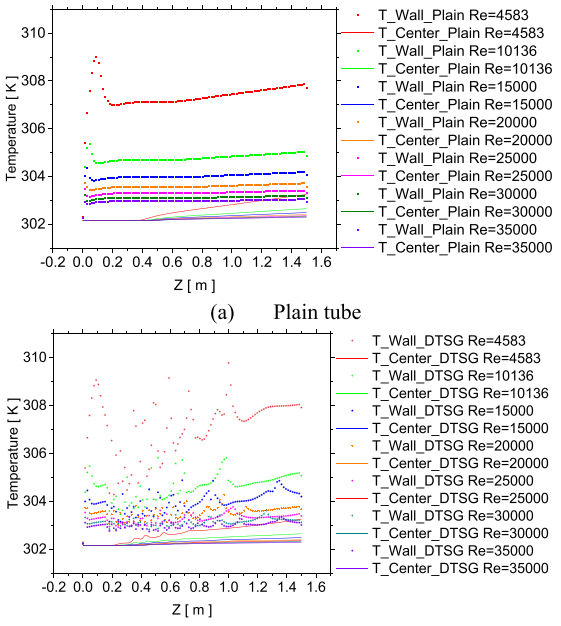


**Fig. 9.** Wall and centerline temperature.

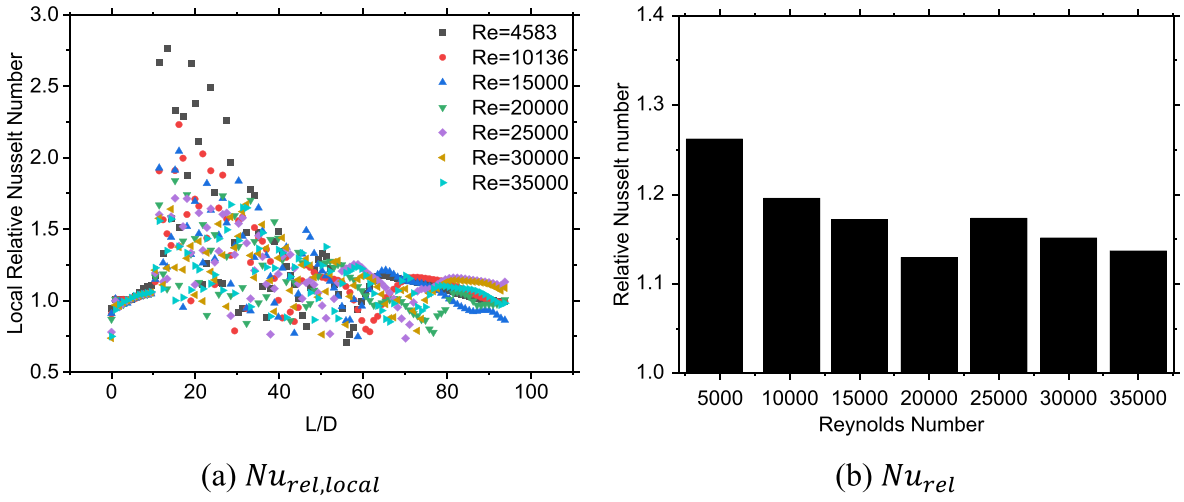


**Fig. 10.** Relative Nusselt number.

gradually. After 1.0 m or L/D = 62.5, the swirling strength almost completely vanished. A similar trend was observed as the Re increased.

Equations 5 and 2 are used to determine *Nu* and $Nu_{rel}$, locally and average using the temperature data from the wall and centerline. Fig. 10 shows the local and average $Nu_{rel}$ for DTS, respectively. Fig. 10a illustrates a scatterplot of 100 points of local $Nu_{rel}$ along the test section. The generated swirling flow along the test section is strongest just after it leaves the DTS, as shown by the local $Nu_{rel}$. The local $Nu_{rel}$ is at peak with 2.77 right after the swirl flow generated at the trailing edge of the DTS. The highest local $Nu_{rel}$ point was achieved at Re of 4583 at the L/D = 13.25. Then, the swirl flow intensity gradually decays as it travels down the tube until the outlet of the tube. The peak local $Nu_{rel}$ decreasing as the Re increasing. The maximum local $Nu_{rel}$ is 1.57 for Re of 35000 at L/D = 14.2. Fig. 10b depicts that when DTS is introduced, *Nu* is enhanced at all Re. In general, the graph demonstrates that the $Nu_{rel}$ is highest at the lowest investigated Re and decreases with Re. The highest average $Nu_{rel}$, 1.26, was discovered at the lowest Re of 4583. On the other hand, the lowest $Nu_{rel}$ was 1.13 at Re 20000. If the $Nu_{rel}$ is determined at a vital swirl flow location or shorter test section, say at L/D = 12.5 to 62.5, the $Nu_{rel}$ increases by up to 12% for Re of 4583, as shown in Table 8. The least increase is 8% for Re 25000 to 35000.

### 3.2.4. *Thermal-hydraulic performance (THP)*

After calculating the $f_{rel}$ and $Nu_{rel}$, the THP can be defined using Equation (1). If the value of THP is greater than unity, a swirler may be utilized as a heat transfer enhancement method for a heat exchanger. Fig. 11 demonstrates the THP of a DTS insert in a heated tube. Similar to $Nu_{rel}$, the maximum THP achieved at the lowest investigated Re with 1.08. The Re of 20000 recorded the THP below the unity, with a value of 0.98. If the THP is computed in the circular tube where the swirl flow is available (L/D = 12.5 to 62.5), the revised THP of DTS inside the heated tube is provided in Table 9. If the heat transfer is investigated for the length of the test section where the swirl flow is strong, the THP may be improved by up to 4% at Re of 4583 and 20000, where now all investigated Re achieved above unity.

## 3.3. *Effect of a diameter of decaying twisted swirler*

As described in Section 2.2, the DTS diameter is set to 15.5 mm, or 3% less than the diameter of the heated tube. Then, in Section 3.2, the performance of the DTS with a diameter of 15.5 mm, an angle of 180°, and 4 blades was examined. This section discusses the generation of swirl flow as the DTS' diameter decreases from 15.5 mm to 13.5 mm by 0.5 mm.

Fig. 12 demonstrates the contour plot of velocity and velocity circumferential of the swirling flow at various DTS diameters. This comparison is for Re of 4583, where the THP of DTS is the greatest. The greater volume of the orange and yellow regions indicates a high value of velocity and velocity circumferential, implying a greater production of swirling flow and, as a result, an increase in the

**Table 8**
Relative Nusselt number at revised tube length.

| Re | Measured from L/D = 12.5–93.75 | Measured from L/D = 12.5–62.5 | Increment of $Nu_{rel}$ (%) |
|---|---|---|---|
| 4583 | 1.26 | 1.42 | 12 |
| 10136 | 1.20 | 1.31 | 9 |
| 15000 | 1.17 | 1.28 | 10 |
| 20000 | 1.13 | 1.25 | 11 |
| 25000 | 1.17 | 1.26 | 8 |
| 30000 | 1.15 | 1.24 | 8 |
| 35000 | 1.14 | 1.23 | 8 |

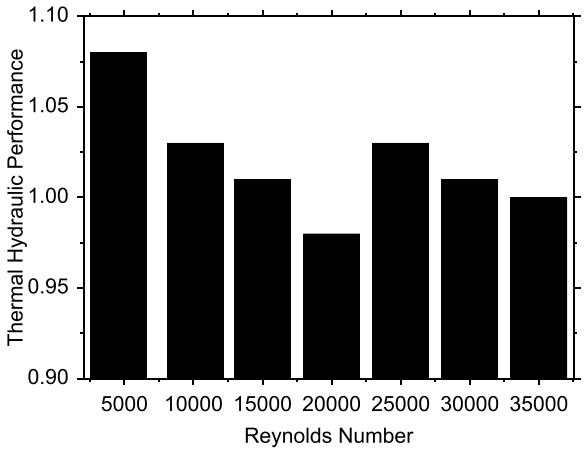


**Fig. 11.** Thermal-hydraulic performance.

**Table 9**
Thermal-hydraulic performance with revised tube lengths.

| Re | Measured from L/D = 12.5–93.75 | Measured from L/D = 12.5–62.5 | Increment of THP (%) |
|---|---|---|---|
| 4583 | 1.08 | 1.12 | 4 |
| 10136 | 1.03 | 1.05 | 2 |
| 15000 | 1.01 | 1.04 | 3 |
| 20000 | 0.98 | 1.02 | 5 |
| 25000 | 1.03 | 1.04 | 2 |
| 30000 | 1.01 | 1.03 | 2 |
| 35000 | 1.00 | 1.02 | 2 |

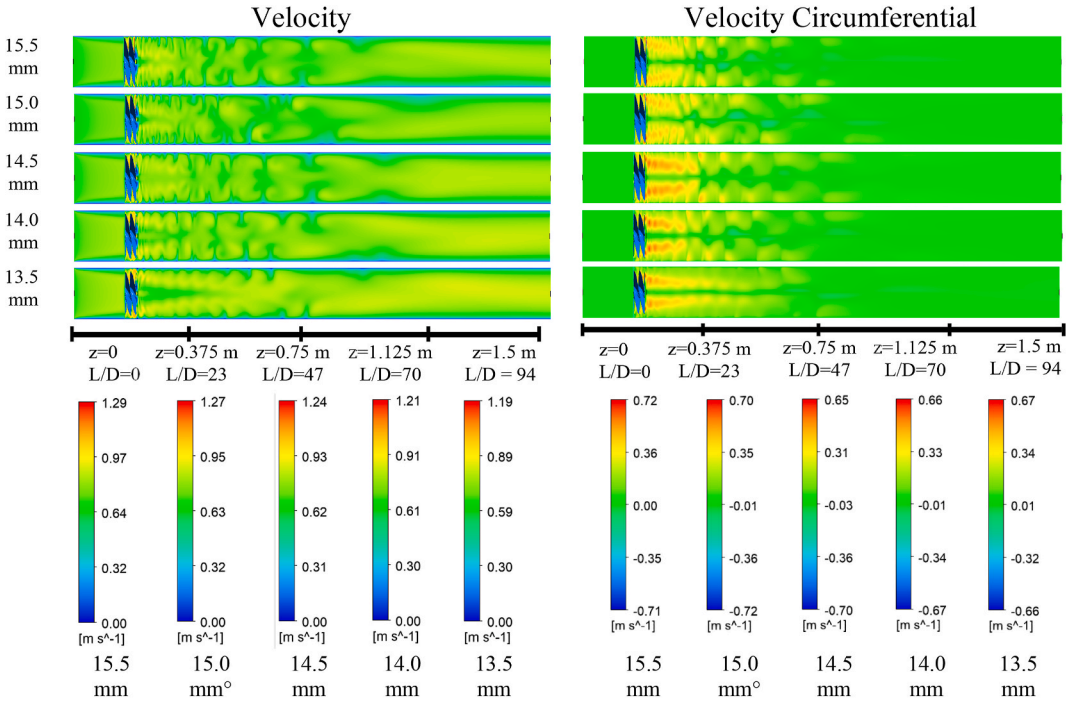


**Fig. 12.** Contour plot of velocity and velocity circumferential for different DTS's diameter (Figure scale x: y: z = 10: 10:1).

heat transfer rate. As presented in the figure, the velocity and velocity circumferential are at their peak as the flow exits the trailing edge of DTS. As described in Section 3.2, the swirl flow lasted until 1 m or L/D = 62.5 when the diameter of the DTS was 15.5 mm. As the diameter decreased, so did the intensity of the swirl. Likewise, the survivability of the swirl flow is diminished. The swirling flow disappears at 0.75 m or L/D = 47 for DTS's 13.5 mm diameter. Comparisons of swirl flow intensity can also be made using the velocity and velocity circumferential ranges generated by each simulation. Maximum velocity and velocity circumferential are generated when the diameter of the DTS is large. Each value is decreased as the diameter of the DTS decreases.

The $Nu_{rel}$ and $f_{rel}$ facilitate the observation of the flow visualization. $Nu_{rel}$ and $f_{rel}$ were calculated by averaging $Nu_{rel,local}$ along the L/D range between 12.5 and 62.5 where swirling flow is present. So, the test section's length is L = 50D or 0.8 m. Fig. 13a demonstrates that as the diameter of the DTS decreases, $Nu_{rel}$ and $f_{rel}$ consistently decrease at the majority of Re investigated. Fig. 13b shows that $f_{rel}$ also decreases with the decreasing of DTS's diameter. The decrease in the value is because of DTS's reduced blockage area. Additionally, both $Nu_{rel}$ and $f_{rel}$ decrease as Re increases. The maximum $Nu_{rel}$ and $f_{rel}$ are 1.41 and 2.00, respectively, when the DTS's diameter is 15.5 mm and Re = 4583.

Hence, THP is measured for the respective DTS's diameter and Re. Fig. 13c shows no profound trend of THP for different diameters of DTS. Nevertheless, the THP is relatively higher at the lowest investigated Re compared to other Re. The maximum THP achieved at the DTS's diameter of 14.5 mm with 1.12. By taking the average $Nu_{rel}$ and THP for all investigated Re, Fig. 13d proves that $Nu_{rel}$ and THP decrease as the diameter decreases. When the diameter is reduced from 15.5 mm to 15.0 mm, the $Nu_{rel}$ value decreases by only 0.5%. As the diameter is reduced further, the $Nu_{rel}$ decreases by 2–3%. As the diameter decreased to 13.5 mm, the $Nu_{rel}$ value decreased by twofold to 7%. In contrast, THP consistently decreases by 1% as the diameter decreases by 0.5 mm, falling below unity at a diameter of 13.5 mm. These results indicate that a diameter of 15.5 mm is optimal for THP DTS.

### 3.4. Effect of twist angle of decaying twisted swirler

With a diameter of 15.5 mm and 4 blades, the effect of the DTS twist angle is investigated. Fig. 14 portrays the contour plot of velocity and velocity circumferential of DTS at twist angles ranging from 0° to 360° with 60° intervals.

Similarly to the previous section, these contour plots are extracted for the Re of 4583, where DTS's THP is highest. Obviously, swirl flow is not generated when the twist angle is 0°. The swirl flow is produced when the twist angle is increased to 60°, resulting in the

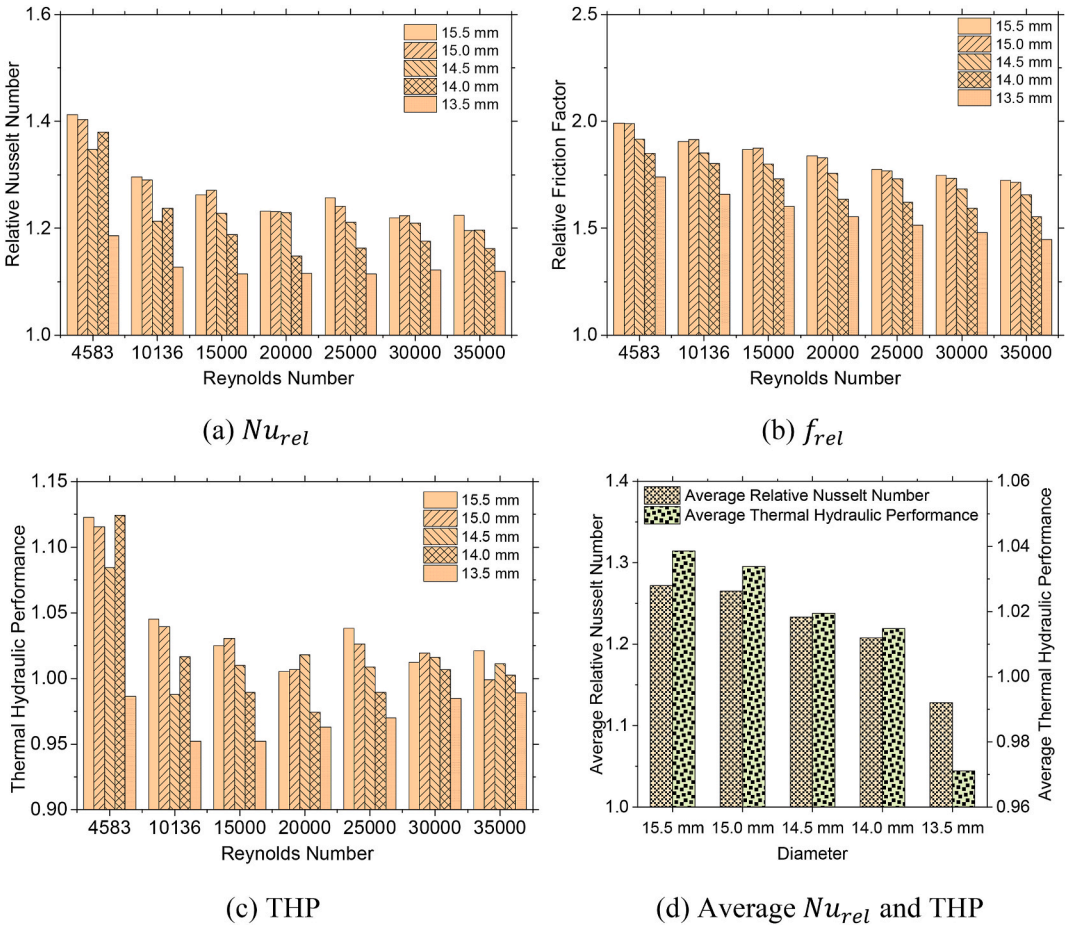


**Fig. 13.** Effect of DTS's diameter on $Nu_{rel}$, $f_{rel}$ and THP.

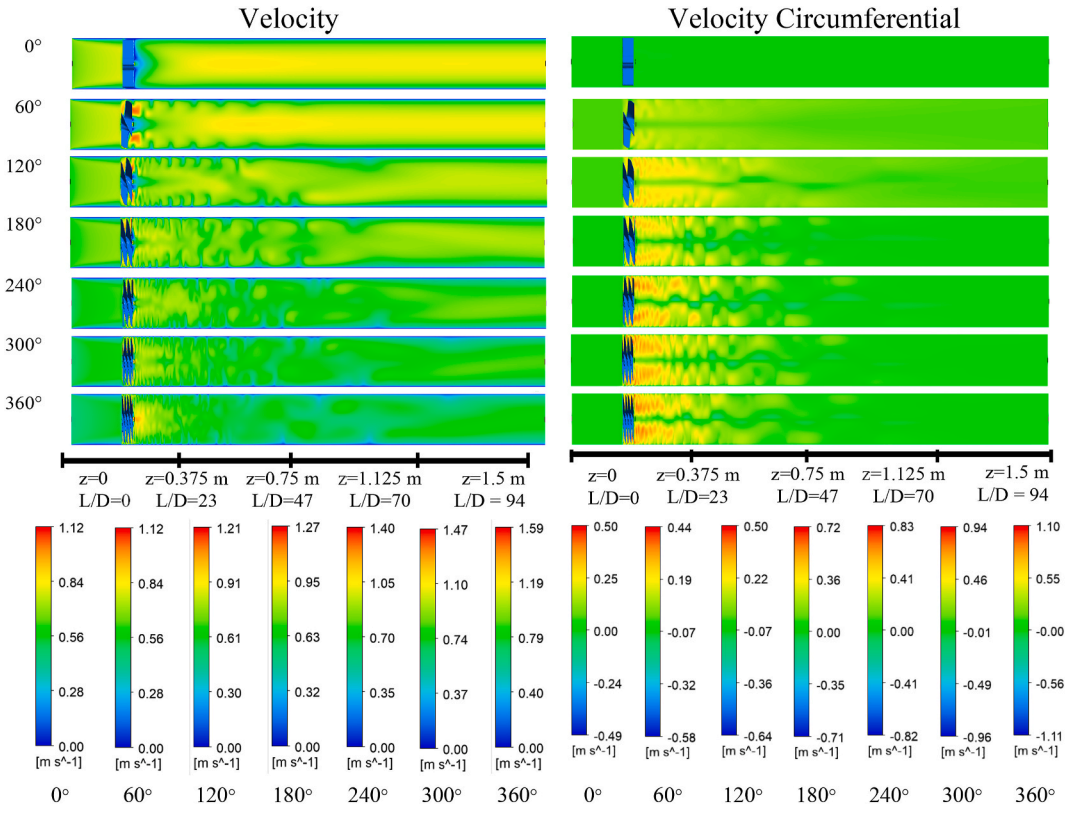


**Fig. 14.** Contour plot of velocity and velocity circumferential for different DTS's twist angle (Figure scale x: y: z = 10: 10:1).

velocity circumferential generation. This velocity gradually decreases until it is resolved after 0.75 m, corresponding to an L/D = 47. As the twist angle increases, the intensity of the swirl flow increases, and the swirl flow's survivability moves further downstream. When the twist angle is 360°, the swirl flow can last for 1.3 m, equivalent to L/D = 81.25.

As shown in Fig. 15a, $Nu_{rel}$ reaches its maximum value at the maximum investigated twist angle. This trend is consistent across all Re that has been investigated. As Re increases, the $Nu_{rel}$ decreases. As the flow enters the leading edge of the DTS, the incoming flow undergoes an immediate change from axial to circumferential flow. The greater the twist angle, the quicker the adjustments must be. Therefore, the higher the swirl flow's intensity. DTS is more effective when the twist angle is 120° or greater as $Nu_{rel}$ multiplies as the twist angle increases from 60° to 120° at the majority Re that has been studied. Hence, DTS achieved the highest $Nu_{rel}$ of 1.65 at Re of 4583 with a twist angle of 360°. The twist angle effect is more noticeable when $Nu_{rel}$ is averaged over all Re investigated, as shown in Fig. 15d. The average $Nu_{rel}$ rises by 9% when the twist angle is increased from 60° to 120°, compared to a 4% increase when the twist angle is increased from 0° to 60°. However, as the twist angle increased from 240° to 300° and then 360°, the average $Nu_{rel}$ increased by only 3%, rendering the twist angle inefficient. On the other hand, $f_{rel}$ consistently increases as the twist angle increases by 60°, as shown in Fig. 15b. As the twist angle grows, the axial flow approaches a greater degree of obstruction. $f_{rel}$ decreases slightly as Re increases. However, the $f_{rel}$ across Re investigated for a twist angle of 360° demonstrates no significant changes.

Fig. 15c demonstrates that, similar to the effect of DRSG diameter, the THP is greatest for the lowest Re investigated. The maximum THP is 1.16 with a twist angle of 300°. Nonetheless, it is difficult to determine the trend of THP as DTS twist angles increase. Therefore, the THP of all Re investigated is averaged. Fig. 15d illustrates that the THP reached its maximum value when the DTS's twist angle was 180° with 1.04. In contrast, the THP equals one when the twist angle is 0° and 300°. Even though a twist angle of 360° generates high intensity of swirling flow and maximum $Nu_{rel}$, THP is below unity, indicating that this angle should not be used as a swirler.

This result does match the investigation of twist angle for a twisted tube with a four-point star swirler conducted by Jafari et al. [29]. The authors examined 90°, 180°, 270°, and 360° turbulators. The swirler's maximum $Nu_{rel}$ and $f_{rel}$ are 1.7 and 1.48 at a twist angle of 360°. The maximum $Nu_{rel}$ was obtained at the lowest investigated Re of 12000 and maximum $f_{rel}$ was obtained at highest Re of 27000. However, the maximum thermal efficiency was achieved at a twist angle of 360° with 1.54. Similar research was conducted by Jumpholkul et al. [28] for free-rotating swirlers with twist angles ranging from 30° to 90°; friction factor and efficiency index were not significantly affected. This result may be accurate because the twist angle is only effective at angles of 120° or greater.

### 3.5. *Effect of blade count of decaying twisted swirler*

As shown in Table 2, the authors have customised their decaying swirler with 4–8 blades. Different blade counts may substantially affect heat transfer and flow obstruction. Since the highest THP is achieved when the twist angle is 180° and 15.5 mm, this parameter

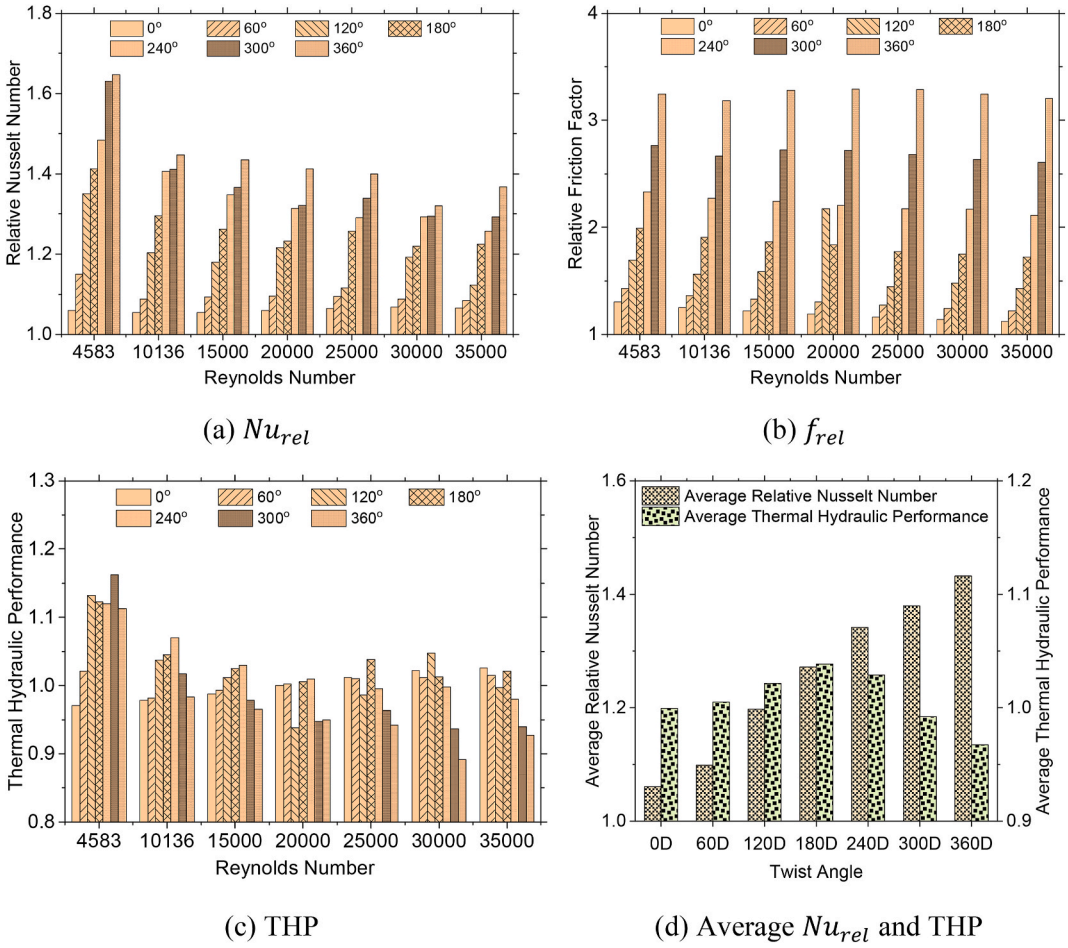


**Fig. 15.** Effect of DTS's twist angle on $Nu_{rel}$, $f_{rel}$ and THP.

determines the optimal blade count for THP. Fig. 16 displays velocity and velocity circumferential contour plots for five different blade counts of DTS in a heated tube. The blade count in the DTS was studied across a spectrum ranging from 2 to 6. These contour plots are also extracted for Re of 4583, where both $Nu_{rel}$ and $f_{rel}$ are at their highest values. As the flow passes through the DTS, the velocity circumferential increases at every blade count. DTS generated greater swirl flow intensity as the blade count increased from 2 to 6. For the 2 blades of the DTS, the swirl flow disappeared after travelling beyond 0.75 m or L/D = 47. The wake region behind the DTS grows, and the blockage effect increases in proportion to the blade count.

Fig. 17a demonstrates that $Nu_{rel}$ is relatively dispersed as the number of blades increases for a given Re. For any given blade count, the histogram indicates that $Nu_{rel}$ in decreases as Re increases. The majority of investigated Re, however, suggests that the $Nu_{rel}$ is maximum for DTS with 6 blades. With 6 blades and a Re of 4583, the highest achievable $Nu_{rel}$ is 1.54. $Nu_{rel}$ is found to be constant for 3 blades ranging from 2 to 4. The $Nu_{rel}$ gradually increases as the blade count increases from 4 to 6. When the $Nu_{rel}$ values are averaged across all the Re investigated, the value does increase with the blade count, as shown in Fig. 17d. Fig. 17b demonstrates that, for a given Re, $f_{rel}$ increases monotonically with increasing blade count, indicating that the flow through the DTS experienced more significant pressure losses. Same to the previous two sections, the $f_{rel}$ decreases as Re increases for any given blade count. With 6 blades and the lowest Re, the maximum $f_{rel}$. was achieved. Adding one DTS blade increases $f_{rel}$. by roughly 10%. As the blade count increases, the surface friction encountered by the incoming flow increases marginally. THP is greatest with 1.17 at the lowest investigated Re with 2 and 6 blades, as shown in Fig. 17c. Nonetheless, the THP scatters as the blade count increases. As a result, the average THP across investigated Re proved that decreasing the number of DTS blades from 4 to 2 at a twist angle of 180° increases THP by 4%, as shown in Fig. 17d. With a DTS diameter of 15.5 mm, 180°, and 2 blades, the THP rises from 1.04 to 1.08. In addition, the histogram demonstrates that all blade count investigated exceeded unity.

Table 10 tabulated the summary of the DTS's diameter, twist angle and blade count that reached the highest average $Nu_{rel}$ and THP.

### 3.6. Comparison with the literature

The performance of DTS with the diameter of 15.5 mm, 2 blades and 180 ° twist angle is further examined by measuring its $Nu_{rel}$ and THP using the same dimensionless length of the test section as is used in the corresponding literature. Swirler's configurations from

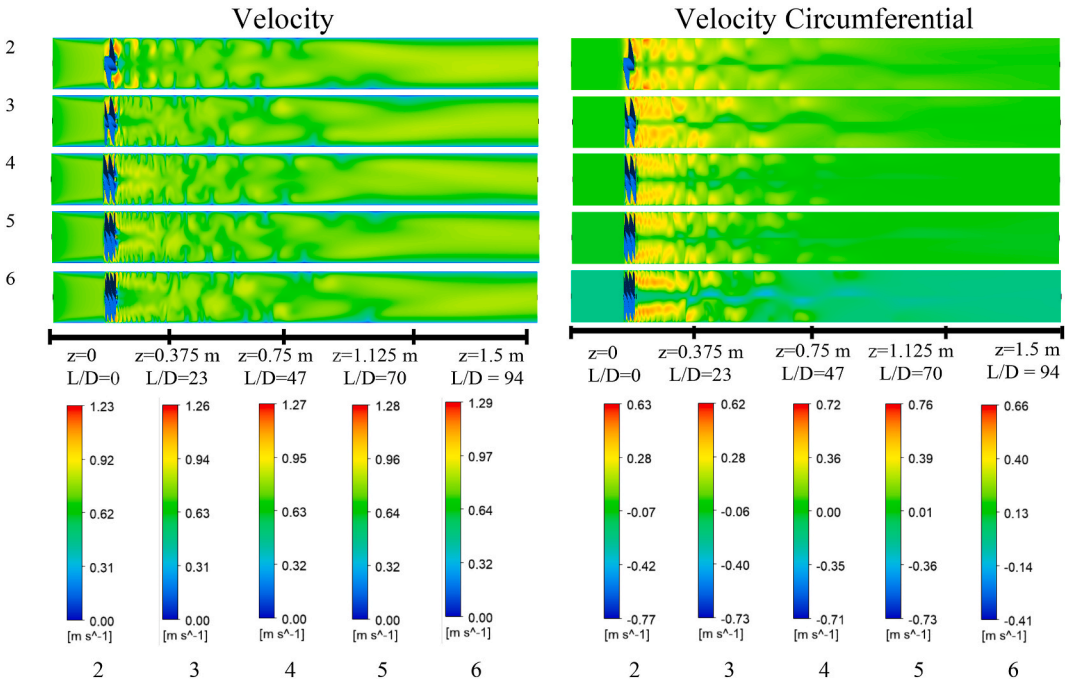


**Fig. 16.** Contour plot of velocity and velocity circumferential for different DTS's blade count (Figure scale x: y: z = 10: 10:1).

the literature with the highest $Nu_{rel}$ and THP values are listed in Table 11. For the analysis, we assume that all literatures have measured the $Nu_{rel}$ from the trailing edge of the decaying swirler to the tube's outlet, where the swirl flow is still strong.

Fig. 18 compares the $Nu_{rel}$ and THP of present work to those in the literature. In the literature, the swirler was investigated for various types of base fluid such as water, air and nanofluid at multiple concentrations and swirler parameters configuration. Nevertheless, only swirler parameter configurations are considered when extracting the $Nu_{rel}$ and THP data. The comparison of the swirlers in Fig. 18a demonstrates that they both exhibit the same trend of $Nu_{rel}$ with respect to Re. The $Nu_{rel}$ is greatest at the lowest Re and decreases with increasing Re. This trend is not the case for Jumpholkul et al. [28]'s free-rotating SG, as the $Nu_{rel}$ scatters as Re increases. Due to the limited range of Re investigated, the result may be unable to discern a significant trend. The comparison reveals that for the same range of Re, the DTS has a higher $Nu_{rel}$ than the other SG at the same dimensionless test section length, except for the four-point star SG by Jafari et al. [29]. This SG has more blades than DTS which contributed to high friction factor. Nonetheless, the twist angle is greater, which may contribute to the stronger swirl flow intensity produced by this SG. With the value of 2.3, the DTS contributed the highest $Nu_{rel}$ at the lowest investigated Re in this comparison.

In contrast, the comparison of THP values in Fig. 18b to $Nu_{rel}$ in Fig. 18a yields different results. Using the same dimensionless length of the test section at the same range of Re, DTS contributed to a lower THP than every other SG, except for the free-rotating swirler. Despite this, the results indicate that the DTS's THP is greater than unity for all test section' lengths. Except for the free-rotating swirler by Jumpholkul et al. [28], the value is highest at the lowest investigated Re and decreases as Re increases. DTS contributed to a high THP at low Re, but as Re increases to 25000 with a shorter test section, it drops dramatically below unity. The DTS's THP is identical to that of the swirler with profiled blades by Indurain et al. [26] for Re lower than 10000. Since DTS has a higher $Nu_{rel}$ than most swirlers but a lower THP, this result indicates that DTS contributed to a significantly higher $f_{rel}$ than other swirlers.

### 3.7. Regression correlation

Equations (8)–(13) provides the regression correlations for the Nusselt number and friction factor of the DTS, considering the parameters of diameter, twist angle, and blade count. The regression models analyzed a dataset consisting of 133 numerical data. These equations are valid for a Reynolds number range of $4583 \leq Re \leq 35{,}000$.

Nusselt number and friction factor regression equations for varying DTS diameters are

$$Nu = 0.0162 Re^{0.8378}\, Pr^{0.4} \left(1 + \frac{D}{15.5}\right)^{0.1981} \tag{8}$$

$$f = 0.736 Re^{-0.3298} \left(1 + \frac{D}{15.5}\right)^{0.9016} \tag{9}$$

These equations are suitable for DTS with twist angle of 180° and 4 blades. The equation is applicable within the diameter range of 13.5 mm–15.5 mm.

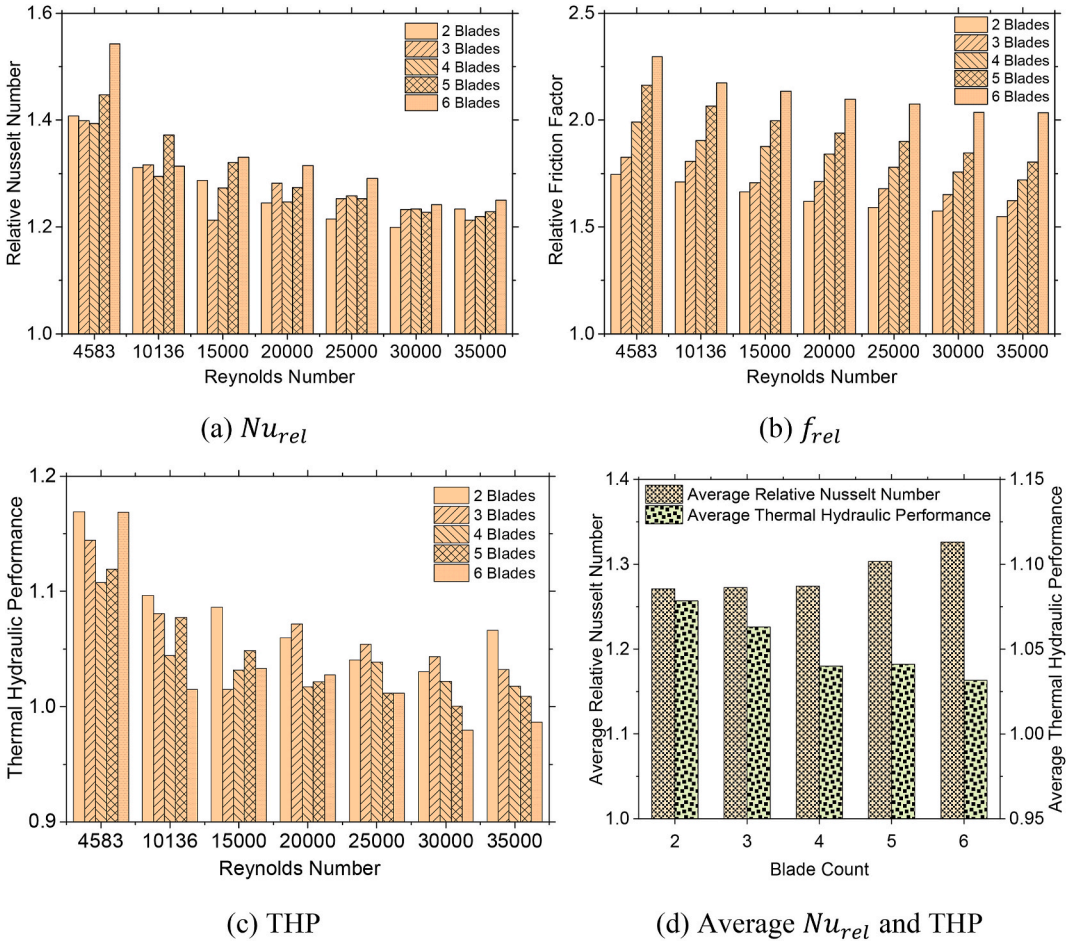


**Fig. 17.** Effect of DTS's blade count on $Nu_{rel}$, $f_{rel}$ and THP.

**Table 10**
Summary of average THP with DTS's parameter investigation.

| Parameter | Range of Parameter | Average $Nu_{rel}$ | | Average THP | |
|---|---|---|---|---|---|
| | | Optimum Parameter | Maximum $Nu_{rel}$ | Optimum Parameter | Maximum THP |
| Diameter | 13.5 mm, 14.0 mm, 14.5 mm, 15.0 mm, 15.5 mm | 15.5 mm | 1.27 | 15.5 mm | 1.04 |
| Twist angle | 0°, 60°, 120°, 180°, 240°, 300°, 360° | 360° | 1.43 | 180° | 1.04 |
| Blade count | 2, 3, 4, 5, 6 | 6 | 1.32 | 2 | 1.08 |

Nusselt number and friction factor regression equations for varying DTS twist angle are

$$Nu = 0.02Re^{0.8186}\ Pr^{0.4}\left(1+\frac{\theta}{360^{\circ}}\right)^{0.3468} \tag{10}$$

$$f = 0.489Re^{-0.289}\left(1+\frac{\theta}{360^{\circ}}\right)^{1.7184} \tag{11}$$

These equations are suitable for DTS with diameter of 15.5 mm and 4 blades. The equation is applicable within the twist angle's range of $0^{\circ} \le \theta \le 360^{\circ}$.

Nusselt number and friction factor regression equations for varying DTS blade count are

$$Nu = 0.01971Re^{0.8228}\ Pr^{0.4}\left(1+\frac{N}{6}\right)^{0.2378} \tag{12}$$

**Table 11**
Swirler configurations.

| Authors | Name of SG | Dimensionless test section length (L/D) | Base fluid | Blade count | Twist angle |
|---|---|---|---|---|---|
| Present paper | Decaying twisted SG | 81.25 | W: EG 60:40% | 2 | 180 ° |
| Jafari et al. [29] | Four-point star SG | 3 | Water | 4 | 360 ° |
| Taheran et al. [30] | 6 blades swirl flow generator | 5 | Ag/Water 0.1 vol % | 6 | 360 ° |
| Indurain et al. [26] | Swirler with profiled blades | 5 | Air | 8 | 40 ° |
| Xu et al. [27] | Winglet vortex generator | 5.38 | Air | 4 | 30 ° and blockage ratio 0.1. |
| Bilen et al. [48] | Decaying swirl generator | 40 | Air | 4 | 50 ° |
| Jumpholkul et al. [28] | Free rotating SG | 281 | Water | 4 | 90 ° |

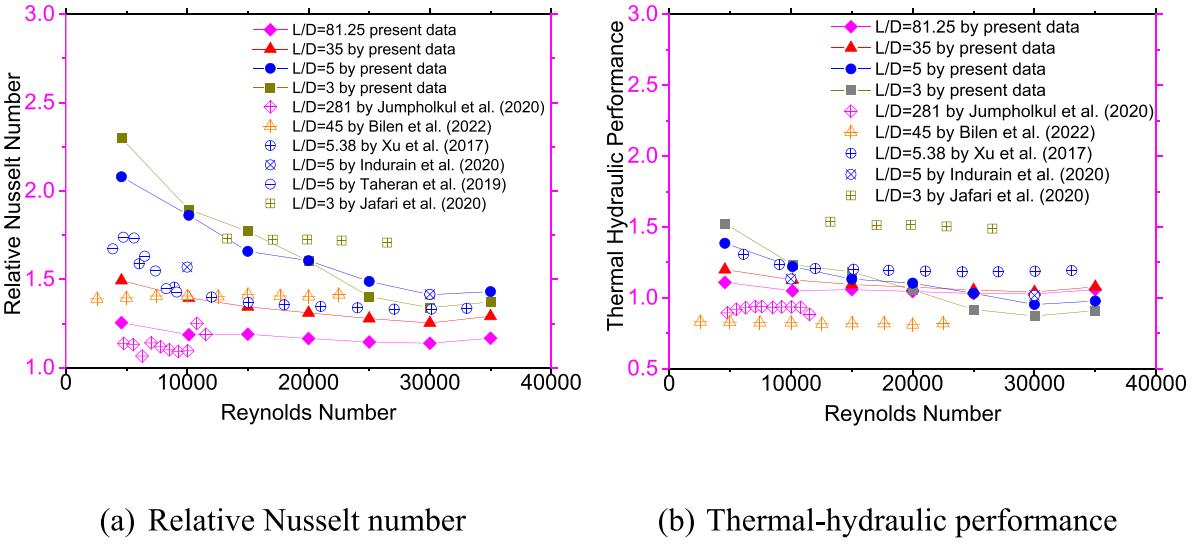


(a) Relative Nusselt number (b) Thermal-hydraulic performance

**Fig. 18.** Comparison with the literature.

**Table 12**
Deviations Statistics of data.

| Parameter | Dimensionless number | Average Deviation (%) | Standard Deviation (%) | Maximum Deviation (%) |
|---|---|---|---|---|
| Diameter | Nusselt number | 2.51 | 1.88 | 6.5 |
| | Friction factor | 4.05 | 3.53 | 11.09 |
| Twist angle | Nusselt number | 1.39 | 1.25 | 4.28 |
| | Friction factor | 4.24 | 2.76 | 9.84 |
| Blade count | Nusselt number | 2.35 | 1.70 | 6.09 |
| | Friction factor | 5.53 | 4.85 | 15.73 |

$$f = 0.763Re^{-0.32125}\left(1+\frac{N}{6}\right)^{0.9419} \tag{13}$$

These equations are suitable for DTS with diameter of 15.5 mm and twist angle of 180°. The equation is applicable within the blade count's range of $2 \leq N \leq 6$.

Table 12 provides the values for the average deviation, standard deviation, and maximum deviation for all regression equations. Fig. 19 confirms a strong agreement between the data obtained from numerical simulation and the predicted data derived from regression correlations.

### 3.8. Further investigation

It has been demonstrated through numerical simulations that DTS can be used to improve heat transfer with low pumping power.

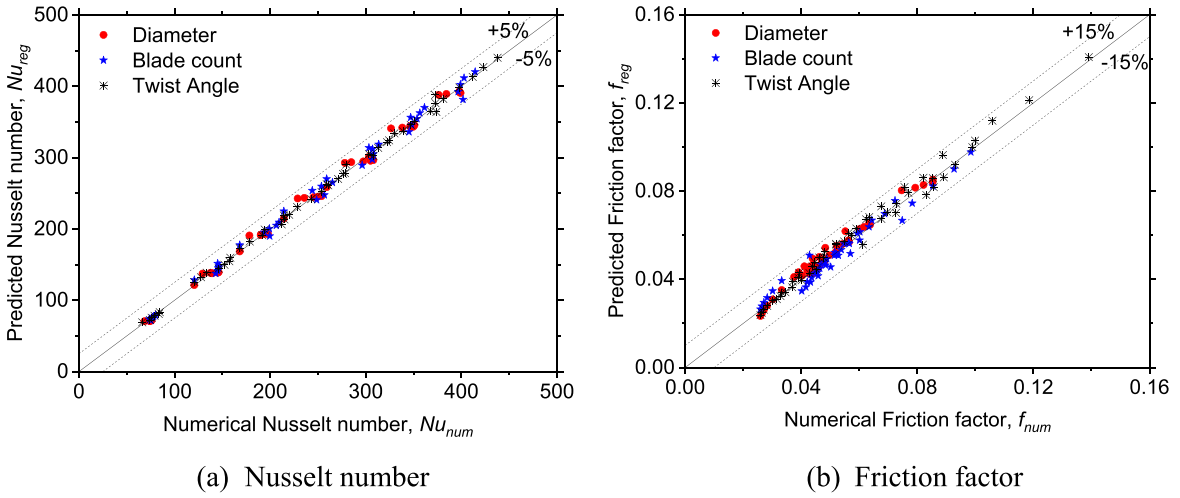


**Fig. 19.** Confirmation of predicted and numerical data for Nusselt number and friction factor.

DTS was designed to produce prototypes on a 3D printer and tested in controlled lab environments. Numerical evidence from the DTS showed that the swirl flow could not persist to the tube's outlet, especially at low Re. Furthermore, the THP of DTS has been demonstrated to be lower when compared to other decaying swirlers in the literature. Thus, thorough critical design analysis is essential. The current DTS design requires some improvements. The design of the DTS was inspired by twisted tape, often employed as a continuous swirler. The blade's basic shape is a twisted rectangle. However, the surface friction may be reduced if the DTS is constructed with a twisted triangle. Although the blade will make less contact with the flow's surface, it will still be able to glide the flow. On the other hand, the length of DTS was chosen to be L/D = 2.25 because L/D = 1 may be insufficient for a 1.5-m-long tube. Despite this, the analysis indicated that the length of the DTS is inadequate for the produced swirl flow to endure till the end of the tube. Consequently, the length of the DTS should be expanded, or the DTS may be inserted in an array or free-rotating configuration. For the swirler to be physically printed, the thickness of the twisted blade must be neither too thick nor too thin. To improve the THP of forced convection heat transfer, the previously listed parameters must be addressed when modifying DTS.

## 4. Conclusions

The thermal-hydraulic performance of the Decaying Twisted Swirler (DTS) was numerically investigated. The investigation focused on Reynolds numbers ranging from 4583 to 35000. The horizontal heated tube with L/D = 93.75 was filled with a working fluid of 60% water and 40% ethylene glycol. The DTS parametric study began with a 15.5 mm diameter, a twist angle of 180°, and 4 blades. At the lowest measured Re of 4583, the highest thermal-hydraulic performance is 1.08. Nevertheless, the swirling flow vanished after 1 m or L/D = 62.5. The maximum thermal-hydraulic performance is increased by 4% to 1.12 in the strong swirl flow region. As a result, this tube length was chosen for further research. When the thermal-hydraulic performance was investigated at the average Re, the value increased as the DTS diameter increased, and the blade count decreased. The thermal-hydraulic performance is maximum when the DTS twist angle is 180°. Thermal-hydraulic performance reaches its greatest value of 1.08 when the DTS diameter is 15.5 mm, the angle is 180°, and 2 blades. The thermal-hydraulic performance can be amplified to increase the intensity and survival of the produced swirl flow by modifying the length, thickness, or array configuration of the DTS.

## CRediT authorship contribution statement

**At-Tasneem Mohd Amin:** Methodology, Validation, Formal analysis, Investigation, Data curation, Visualization, Project administration, Funding acquisition, Writing - original draft, Writing - review & editing. **Wan Azmi Wan Hamzah:** Conceptualization, Resources, Supervision, Data curation, Methodology, Validation, Writing - review & editing. **Mohd Azmi Ismail:** Methodology, Software, Supervision, Data curation, Formal analysis, Validation, Writing - review & editing.

## Declaration of competing interest

The authors declare that they have no known competing financial interests or personal relationships that could have appeared to influence the work reported in this paper.

## Data availability

Data will be made available on request.

## Acknowledgement

The authors would like to thank Universiti Malaysia Pahang Al-Sultan Abdullah, Malaysia for financial support under Internal Research grant RDU230313.

## References

[1] S. Javed, H.M. Ali, H. Babar, M.S. Khan, M.M. Janjua, M.A. Bashir, Internal convective heat transfer of nanofluids in different flow regimes: a comprehensive review, Phys. A Stat. Mech. its Appl. 538 (2020), 122783, https://doi.org/10.1016/j.physa.2019.122783.
[2] S.K. Saha, H. Ranjan, M.S. Emani, A.K. Bharti, Heat transfer fundamentals for design of heat transfer enhancement devices, SpringerBriefs Appl. Sci. Technol. (–16) (2020) 1, https://doi.org/10.1007/978-3-030-20740-3_1.
[3] S. Ahmad, S. Abdullah, K. Sopian, A review on the thermal performance of nanofluid inside circular tube with twisted tape inserts, Adv. Mech. Eng. 12 (6) (2020), https://doi.org/10.1177/1687814020924893.
[4] R. Andrzejczyk, T. Muszynski, P. Kozak, Experimental investigation on straight and u-bend double tube heat exchanger with active and passive enhancement methods, MATEC Web Conf 240 (2018), https://doi.org/10.1051/matecconf/201824002001.
[5] W. Grassi, D. Testi, M. Saputelli, EHD enhanced heat transfer in a vertical annulus, Int. Commun. Heat Mass Tran. 32 (6) (2005) 748–757, https://doi.org/10.1016/j.icheatmasstransfer.2004.10.011.
[6] C. Nuntadusit, M. Wae-hayee, A. Bunyajitradulya, S. Eiamsa-ard, Visualisation and heat transfer characteristics for swirling impinging jet, Int. Commun. Heat Mass Tran. 39 (5) (2012) 640–648, https://doi.org/10.1016/j.icheatmasstransfer.2012.03.002.
[7] S. Tian, M. Barigou, An improved vibration technique for enhancing temperature uniformity and heat transfer in viscous fluid flow, Chem. Eng. Sci. 123 (2015) 609–619, https://doi.org/10.1016/j.ces.2014.11.029.
[8] O. Guven, M.K. Aktas, Y. Bayazitoglu, Experimental investigation of oscillation controlled thermal, in: Proceedings of the ASME 2016 Heat Transfer Summer Conference, 2017, pp. 1–7.
[9] A. Moosavi, M. Abbasalizadeh, H. Sadighi Dizaji, Optimisation heat transfer and pressure drop characteristics via air bubble injection inside a shell and coiled tube heat exchanger, Exp. Therm. Fluid Sci. 78 (2016) 1–9, https://doi.org/10.1016/j.expthermflusci.2016.05.011.
[10] G. Srinivasa Rao, V. Subha, S. Jagan Raj, S. Farrukh Rasheed, M. Rashmi, K. Suganandam, Thermo-hydraulic performance of nanofluids composed of functionalized MWCNT, Mater. Today: Proc. (2023), https://doi.org/10.1016/j.matpr.2023.08.084.
[11] M. Awais, et al., Heat transfer and pressure drop performance of Nanofluid: a state-of- the-art review, Int. J. Thermofluids 9 (2021) 1–21, https://doi.org/10.1016/j.ijft.2021.100065.
[12] A. Kaood, M.A. Hassan, Thermo-hydraulic performance of nanofluids flow in various internally corrugated tubes, Chem. Eng. Process: Process Intensif. 154 (2020), https://doi.org/10.1016/j.cep.2020.108043.
[13] I. Zakaria, W.A.N.W. Mohamed, W.H. Azmi, A.M.I. Mamat, R. Mamat, W.R.W. Daud, Thermo-electrical performance of PEM fuel cell using $Al_2O_3$ nanofluids, Int. J. Heat Mass Tran. 119 (2018) 460–471, https://doi.org/10.1016/j.ijheatmasstransfer.2017.11.137.
[14] M. Kh Abdolbaqi, R. Mamat, N.A.C. Sidik, W.H. Azmi, P. Selvakumar, Experimental investigation and development of new correlations for heat transfer enhancement and friction factor of BioGlycol/water based TiO2 nanofluids in flat tubes, Int. J. Heat Mass Tran. 108 (2017) 1026–1035, https://doi.org/10.1016/j.ijheatmasstransfer.2016.12.024.
[15] S.D. Shelare, K.R. Aglawe, P.N. Belkhode, A review on twisted tape inserts for enhancing the heat transfer, Mater. Today: Proc. 54 (2022) 560–565, https://doi.org/10.1016/j.matpr.2021.09.012.
[16] O. Keklikcioglu, V. Ozceyhan, A review of heat transfer enhancement methods using coiled wire and twisted tape inserts, in: Heat Transfer - Models, Methods and Applications, InTech, 2018, https://doi.org/10.5772/intechopen.74516.
[17] N.A. Lokhande, M.S. Basavaraj, Heat Transfer in Round Tube Using Conical Ring Inserts: A Review", 2015 [Online]. Available: https://api.semanticscholar.org/CorpusID:114068715.
[18] S. Liu, M. Sakr, A comprehensive review on passive heat transfer enhancements in pipe exchangers, Renew. Sustain. Energy Rev. 19 (2013) 64–81, https://doi.org/10.1016/j.rser.2012.11.021.
[19] S.K. Saha, H. Ranjan, M.S. Emani, A.K. Bharti, Swirlers, extended surface insert and tangential injection devices, SpringerBriefs Appl. Sci. Technol. (2020) 83–97, https://doi.org/10.1007/978-3-030-20776-2_4.
[20] A.O. Firoozi, S. Majidi, M. Ameri, A numerical assessment on heat transfer and flow characteristics of nanofluid in tubes enhanced with a variety of dimple configurations, Therm. Sci. Eng. Prog. 19 (2020), https://doi.org/10.1016/j.tsep.2020.100578.
[21] E. Bellos, C. Tzivanidis, D. Tsimpoukis, Enhancing the performance of parabolic trough collectors using nanofluids and turbulators, Renew. Sustain. Energy Rev. 91 (2018) 358–375, https://doi.org/10.1016/j.rser.2018.03.091.
[22] A. Boonloi, W. Jedsadaratanachai, Numerical assessments of flow pattern and heat transfer profile for the round tube equipped with different configurations of the dual-inclined baffle, Case Stud. Therm. Eng. 27 (2021), https://doi.org/10.1016/j.csite.2021.101242.
[23] J. Heeraman, R. Kumar, P.K. Chaurasiya, H. Ivanov Beloev, I. Krastev Iliev, Experimental evaluation and thermal performance analysis of a twisted tape with dimple configuration in a heat exchanger, Case Stud. Therm. Eng. 46 (2023), https://doi.org/10.1016/j.csite.2023.103003.
[24] V.H. Harish, K. Manjunath, Heat and fluid flow behaviors in a laminar tube flow with circular protruded twisted tape inserts, Case Stud. Therm. Eng. 32 (2022), https://doi.org/10.1016/j.csite.2022.101880.
[25] S. Saedodin, M. Zaboli, S.H. Rostamian, Effect of twisted turbulator and various metal oxide nanofluids on the thermal performance of a straight tube: numerical study based on experimental data, Chem. Eng. Process. - Process Intensif. 158 (2020), https://doi.org/10.1016/j.cep.2020.108106.
[26] B. Indurain, F. Beaubert, S. Lalot, D. Uystepruyst, Computational fluid dynamics investigation of the thermal performances of a swirler with profiled blades, Heat Tran. Eng. 7632 (2020), https://doi.org/10.1080/01457632.2020.1800271.
[27] Y. Xu, M.D. Islam, N. Kharoua, Numerical study of winglets vortex generator effects on thermal performance in a circular pipe, Int. J. Therm. Sci. 112 (2017) 304–317, https://doi.org/10.1016/j.ijthermalsci.2016.10.015.
[28] C. Jumpholkul, et al., Experimental investigation of the heat transfer and pressure drop characteristics of SiO2/water nanofluids flowing through a circular tube equipped with free rotating swirlers, Heat Mass Tran. 56 (5) (2020) 1613–1626, https://doi.org/10.1007/s00231-019-02782-z.
[29] M. Jafari, A. Farajollahi, H. Gazori, The experimental investigation concerning the heat transfer enhancement via a four-point star swirler in the presence of water–ethylene glycol mixtures, J. Therm. Anal. Calorim. (2020), https://doi.org/10.1007/s10973-020-09408-1.
[30] E. Taheran, K. Javaherdeh, Experimental and numerical study on the thermal and hydrodynamic characteristics of non-Newtonian decaying swirl flows, J. Dispersion Sci. Technol. 40 (9) (2019) 1288–1299, https://doi.org/10.1080/01932691.2018.1510783.
[31] W.H. Azmi, K. Abdul Hamid, A.I. Ramadhan, A.I.M. Shaiful, Thermal-hydraulic performance for hybrid composition ratio of TiO2-SiO2 nanofluids in a tube with wire coil inserts, Case Stud. Therm. Eng. 25 (2021), https://doi.org/10.1016/j.csite.2021.100899.
[32] A.O. Firoozi, S. Majidi, M. Ameri, A numerical assessment on heat transfer and flow characteristics of nanofluid in tubes enhanced with a variety of dimple configurations, Therm. Sci. Eng. Prog. 19 (2020), https://doi.org/10.1016/j.tsep.2020.100578.
[33] J. Du, Y. Hong, Experimental investigation on thermal-hydraulic characteristics in a traverse rib tube fitted with regularly spaced helical tapes, Int. J. Heat Mass Tran. 154 (2020), https://doi.org/10.1016/j.ijheatmasstransfer.2020.119726.
[34] E. Bellos, C. Tzivanidis, D. Tsimpoukis, Enhancing the performance of parabolic trough collectors using nanofluids and turbulators, Renew. Sustain. Energy Rev. 91 (2018) 358–375, https://doi.org/10.1016/j.rser.2018.03.091.
[35] P. Liu, N. Zheng, F. Shan, Z. Liu, W. Liu, Numerical study on characteristics of heat transfer and friction factor in a circular tube with central slant rods, Int. J. Heat Mass Tran. 99 (2016) 268–282, https://doi.org/10.1016/j.ijheatmasstransfer.2016.03.059.

[36] N. Zheng, P. Liu, F. Shan, Z. Liu, W. Liu, Effects of rib arrangements on the flow pattern and heat transfer in an internally ribbed heat exchanger tube, Int. J. Therm. Sci. 101 (2016) 93–105, https://doi.org/10.1016/j.ijthermalsci.2015.10.035.
[37] W. Jedsadaratanachai, N. Jayranaiwachira, P. Promvonge, 3D numerical study on flow structure and heat transfer in a circular tube with V-baffles, Chin. J. Chem. Eng. 23 (2) (2015) 342–349, https://doi.org/10.1016/j.cjche.2014.11.006.
[38] P. Promvonge, N. Koolnapadol, M. Pimsarn, C. Thianpong, Thermal performance enhancement in a heat exchanger tube fitted with inclined vortex rings, Appl. Therm. Eng. 62 (1) (2014) 285–292, https://doi.org/10.1016/j.applthermaleng.2013.09.031.
[39] L.H.K. Goh, Y.M. Hung, G.M. Chen, C.P. Tso, Entropy generation analysis of turbulent convection in a heat exchanger with self-rotating turbulator inserts, Int. J. Therm. Sci. 160 (2021), https://doi.org/10.1016/j.ijthermalsci.2020.106652.
[40] P. Liu, Z. Dong, J. Lv, F. Shan, Z. Liu, W. Liu, Numerical study on thermal-hydraulic performance and exergy analysis of laminar oil flow in a circular tube with fluid exchanger inserts, Int. J. Therm. Sci. 153 (2020), https://doi.org/10.1016/j.ijthermalsci.2020.106365.
[41] M. Pourramezan, H. Ajam, M.A. Raoufi, A. Abadeh, Performance evaluation and optimization of design parameters for twisted conical strip inserts in tubular laminar flow Using Taguchi approach, Int. J. Therm. Sci. 152 (2020), https://doi.org/10.1016/j.ijthermalsci.2020.106324.
[42] M.E. Nakhchi, J.A. Esfahani, K.C. Kim, Numerical study of turbulent flow inside heat exchangers using perforated louvered strip inserts, Int. J. Heat Mass Tran. 148 (2020), https://doi.org/10.1016/j.ijheatmasstransfer.2019.119143.
[43] R. Mashayekhi, H. Arasteh, D. Toghraie, S.H. Motaharpour, A. Keshmiri, M. Afrand, Heat transfer enhancement of Water-Al2O3 nanofluid in an oval channel equipped with two rows of twisted conical strip inserts in various directions: a two-phase approach, Comput. Math. Appl. 79 (8) (2020) 2203–2215, https://doi.org/10.1016/j.camwa.2019.10.024.
[44] M. Bahiraei, N. Mazaheri, M.R. Daneshyar, CFD analysis of second law characteristics for flow of a hybrid biological nanofluid under rotary motion of a twisted tape: exergy destruction and entropy generation analyses, Powder Technol. 372 (2020) 351–361, https://doi.org/10.1016/j.powtec.2020.06.003.
[45] A. Alimoradi, M. Fatahi, S. Rehman, M. Khoshvaght-Aliabadi, S.M. Hassani, Effects of transversely twisted-turbulators on heat transfer and pressure drop of a channel with uniform wall heat flux, Chem. Eng. Process. - Process Intensif. 154 (2020), https://doi.org/10.1016/j.cep.2020.108027.
[46] T. Yan, J. Qu, X. Sun, Y. Chen, Q. Hu, W. Li, Numerical evaluation on the decaying swirling flow in a multi-lobed swirler, Eng. Appl. Comput. Fluid Mech. 14 (1) (2020) 1198–1214, https://doi.org/10.1080/19942060.2020.1816494.
[47] A. Nikoozadeh, A. Behzadmehr, S. Payan, Numerical investigation of turbulent heat transfer enhancement using combined propeller-type turbulator and nanofluid in a circular tube, J. Therm. Anal. Calorim. 140 (3) (2020) 1029–1044, https://doi.org/10.1007/s10973-019-08578-x.
[48] K. Bilen, N. Tokgoz, İ. Solmaz, T. Balta, Thermo-hydraulic performance of tube with decaying swirl flow generators, Appl. Therm. Eng. 200 (Jan. 2022), https://doi.org/10.1016/j.applthermaleng.2021.117643.
[49] K. Abdul Hamid, W.H. Azmi, R. Mamat, K.V. Sharma, Heat transfer performance of TiO2–SiO2 nanofluids in a tube with wire coil inserts, Appl. Therm. Eng. 152 (2019) 275–286, https://doi.org/10.1016/j.applthermaleng.2019.02.083.
[50] S. Ahmad, S. Abdullah, K. Sopian, A review on the thermal performance of nanofluid inside circular tube with twisted tape inserts, Adv. Mech. Eng. 12 (6) (2020), https://doi.org/10.1177/1687814020924893.
[51] W.H. Azmi, N.A. Usri, R. Mamat, K. V Sharma, M.M. Noor, Force convection heat transfer of $Al_2O_3$ nanofluids for different based ratio of water: ethylene glycol mixture, Appl. Therm. Eng. 112 (2017) 707–719, https://doi.org/10.1016/j.applthermaleng.2016.10.135.
[52] ASHRAE Handbook - Fundamental (SI Edition), American Society of Hearing, Refrigerating and Air-Conditioning Engineers Inc., Atlanta, GA, 2009.
[53] B.E. Launder, Second-moment closure: present and future?, 10(4), 1989.
[54] L. Merlier, F. Kuznik, G. Rusaouën, J. Hans, An adapted steady RANS RSM wall-function for building external convection, Build. Environ. 94 (2015) 654–664, https://doi.org/10.1016/j.buildenv.2015.10.010.
[55] T. Yan, J. Qu, X. Sun, Y. Chen, Q. Hu, W. Li, Numerical evaluation on the decaying swirling flow in a multi-lobed swirl generator, Eng. Appl. Computat. Fluid Mech. 14 (1) (2020) 1198–1214, https://doi.org/10.1080/19942060.2020.1816494.
[56] ANSYS, ANSYS Fluent User's Guide, Release 19.0", Equation (6.88), 2018.
[57] G. Hu, Z. Cao, M. Hopkins, J.G. Lyons, M. Brennan-Fournet, D.M. Devine, Nanofillers can be used to enhance the thermal conductivity of commercially available SLA resins, Procedia Manuf. 38 (2019) 1236–1243, https://doi.org/10.1016/j.promfg.2020.01.215.
[58] H. Blasius, Das Aehnlichkeitsgesetz bei Reibungsvorgängen in Flüssigkeiten, Mitteilungen über Forschungsarbeiten auf dem Gebiete des Ingenieurwesens 131 (1913) 1–41 [Interaktyvus]. Available at: http://link.springer.com/10.1007/978-3-662-02239-9.
[59] B.S. Pettukhov, Heat transfer and friction in turbulent pipe flow with variable physical properties, Adv. Heat Tran. 6 (1970) 503–564.
[60] J.M. C, R.H.T. Yunus A Cengel, Fundamental of Thermal-Fluid Sciences, McGraw Hill, New York, 2012.
[61] F.W. Dittus, L.M.K. Boelter, Heat transfer in automobile radiators of the tubular type, Int. Commun. Heat Mass Tran. 12 (1) (1985) 3–22, https://doi.org/10.1016/0735-1933(85)90003-X.
[62] V. Gnielinski, On heat transfer in tubes, Int. J. Heat Mass Tran. 63 (2013) 134–140, https://doi.org/10.1016/j.ijheatmasstransfer.2013.04.015.